population did not always appear to be conserved in the examined cells.

The standard used to evaluate tumor-initiating activity maintains that the candidate cell populations should be able to initiate serially transplantable tumor development. Therefore, we determined and compared the tumor-initiating capacities of $CD133^+$ MRTK cells in NOD/SCID mice (Table 1). As few as 1,000 $CD133^+$ MRTK cells initiated tumor development by 21 days (60-100%), although the same number of $CD133^-$ MRTK cells could not form tumors (0%). Representative serial tumor development in JMU-RTK-1 and JMU-RTK-2 cells is shown in Fig. 4A. Tumor formation was microscopically confirmed in JMU-RTK-1 cells (Fig. 4B). Thus, these results show that MRTK-initiating cells are defined by CD133 expression and that a limited population of $CD133^+$ MRTK-initiating cells can be maintained in culture conditions on plastic dishes. When injected at 1,000 and 10,000 cells, JMU-RTK-1 and JMU-RTK-2 cells formed tumors rapidly (Fig. 4C and D), suggesting that the tumor-initiating potential in JMU-RTK-1 and JMU-RTK-2 cells is higher than that in G401, SWT-1, and SWT-2 cells.

CXCR4 expression in $CD133^+$ MRTK-initiating cells. Our data (see Fig. 2B) suggest that some MRTKs possess marked tendency for distant organ metastasis. Moreover, recent emerging evidence suggests a potential role of the chemokine receptor CXCR4 in tumor-initiating cells and tumor metastasis (9). Therefore, in an effort to determine the correlation between $CD133^+$ MRTK-initiating cells and CXCR4 expression, Western blot analysis using anti-human CXCR4 was done before and after CD133 enrichment in the MRTK cell lines (Fig. 5A). Although unsorted cells expressed CXCR4, some of the cell lines showed increased CXCR4 expression following $CD133^+$ enrichment. Furthermore, fluorescence-activated cell sorting analysis showed cell surface expression of CXCR4 (Fig. 5B), whereas $CD133^-$ cells showed moderate expression of CXCR4.

To determine the metastatic potential in CD133-enriched MRTK cells, orthotopic injection into the left kidney (1,000 cells) was done using $CD133^+$ luciferase-expressing MRTK cells. Although substantial tumor-derived photons were observed at the injection site (data not shown), the resulting metastatic frequency was less correlated with CXCR4 expression levels (Fig. 5C). Thus, some $CD133^+$ MRTK-initiating cells maintained their metastatic potential and the $CD133^-CXCR4^+$ population appeared to play an auxiliary role in tumorigenicity and metastasis.

Table 1. Tumorigenicity of $CD133^+$ MRTK cells in NOD/SCID mice

Cell lines	Cell number	Tumor incidence	
		$CD133^+$	$CD133^-$
JMU-RTK-1	100,000	ND	1/9 (11%)
	10,000	8/9 (89%)*	1/9 (11%)
	1,000	6/9 (67%)*	0/9 (0%)
JMU-RTK-2	100,000	ND	1/6 (17%)
	10,000	4/6 (67%)*	0/6 (0%)
	1,000	4/6 (67%)*	0/6 (0%)
G401	100,000	ND	2/6 (33%)
	10,000	6/6 (100%)*	1/6 (17%)
	1,000	5/6 (80%)*	0/6 (0%)
SWT-1	100,000	ND	1/6 (17%)
	10,000	4/6 (67%)*	0/6 (0%)
	1,000	3/6 (50%)*	0/6 (0%)
SWT-2	100,000	ND	0/6 (0%)
	10,000	4/6 (67%)*	0/6 (0%)
	1,000	4/6 (67%)*	0/6 (0%)
FRTK-1	100,000	ND	3/6 (50%)
	10,000	6/6 (100%)*	1/6 (17%)
	1,000	6/6 (100%)*	0/6 (0%)

NOTE: Cells were injected into the flanks of NOD/SCID mice at the indicated numbers.
Abbreviation: ND, not determined.
*$P < 0.05$ ($CD133^+$ versus $CD133^-$), Fisher's test.

Discussion

We showed that tumorigenic MRTK cells are included in a rare population that expresses CD133. The remarkable features presented in this study include the following: (*a*) the characteristic metastatic fate of MRTK cells in an orthotopic xenotransplantation model of SCID mice; (*b*) $CD133^-$ MRTK cells may play an auxiliary role in tumorigenicity and metastasis.

MRTK cells represent a most progressive rare malignancy of infantile cancers with uncertain histogenesis (11, 12, 15). However, the precise mechanism by which MRTK cells progress is a major interest in cancer biology. Using recent *in vivo* luminescent technology (24, 25), luciferase-labeled MRTK cell lines were used to elucidate the metastatic fate in an orthotopic xenotransplantation model of NOD/SCID mice. Tumor-burdened mice also showed progressiveness in MRTK with distant organ metastasis observed, such as occurred in the liver and lung, in addition to direct invasion of some nearby organs. Thus, these genetically modified transplantable cell lines that were established should provide a useful animal model for the future therapeutic treatment of refractory MRTK.

CD133 was initially described as a surface antigen (a transmembrane pentaspan protein) specific to hematopoietic stem cells (26, 27). Although the biological function of CD133 remains unknown, CD133 is recognized as a stem cell marker for normal and cancerous tissues. In a number of recent studies, monoclonal antibodies against CD133 have been used for the identification and isolation of a putative cancer stem cell population from malignant tumors of brain (6), colon (7, 8), pancreas (9), prostate (10), liver (28, 29), and lung (30). However, our data from the investigation of MRTK cells showed that CD133 expression remains transient and rare even following enrichment using CD133 mAbs. As shown for normal hematopoietic and endothelial progenitors, CD133 expression is limited in early progenitors and usually not detected upon differentiation (26, 27). The present data are consistent with the findings from normal and cancer stem cells as $CD133^+$ subpopulations are exclusively tumorigenic, possess self-renewal capacity, and can differentiate into $CD133^-$ transit-amplifying tumor cells.

Shmelkov et al. (31) also reported that CD133 might not be a suitable marker for colon cancer stem cells. This was elegantly shown using transgenic mice expressing LacZ under control of the CD133 promoter. At least in MRTK, $CD133^+$

cells bore definite tumorigenicity and our data suggest that $CD133^-$ cells may cooperate with $CD133^+$ MRTK cells in terms of tumorigenicity. In human cancers, much evidence has accumulated to provide the consensus that CD133 is a reliable stem cell marker in human cancer specimens. With regard to CD133 expression, it has been shown that seven CD133 mRNA isoforms are controlled by five alternative promoters in a tissue/organ-dependent manner (32). This rather complicated *CD133* gene expression appears to require short-term CD133 expression to retain the organ-specific stem cells. Therefore, further analysis of CD133 transcriptional regulation may provide clues as to how cancer stem cells are regulated between self-renewal and differentiation.

Recent data suggest that the interaction between chemokines and their receptors are also critical components in the regulation of tumor progression and metastasis in many cancer types (33, 34) and that the CXCR4/SDF-1 pathway is involved in the metastatic process of melanoma (17, 34), glioblastoma (35), and colon (36) and pancreatic (37) carcinomas. In fact, clinical studies investigating poor patient prognosis and CXCR4 expression in tumor cells showed a significant correlation for some of the aforementioned malignancies (38-40). Moreover, in the case of pancreatic carcinomas, Hermman et al. (9) showed an important correlation between CXCR4 and CD133 in cancer stem cells, in that a subpopulation of migrating $CXCR4^+CD133^+$ cells is essential for tumor metastasis. Our data (Fig. 5) showed that both $CD133^+$ and $CD133^-$ populations showed CXCR4 expression, thus not entirely consistent with the above report. Our data suggest rather that $CXCR4^+CD133^-$ cells may also contribute to metastatic tumor growth. In this regard, Dalerba and Clarke (41) recently proposed possible models for metastasis-promoting cancer cells, in which $CXCR4^+$ cancer cells act in an auxiliary manner (not unlike the role of macrophages in several tumor model systems; refs. 42, 43). Our data appear to support this proposal. Furthermore, Burns et al. (44) recently reported that an alternate receptor, CXCR7 (RDC1), is expressed in some tumor cells and binds with high affinity to SDF-1. Unlike many other chemokine receptors, ligand activation of CXCR7 does not sufficiently induce migration in tumor cell lines (44) but provides cells with a growth and survival advantage (44-46). Therefore, we speculate that other chemokine receptors may also play a role in the growth and survival advantage of MRTK cells.

Given that MRTK is a progressive malignancy with a poor prognosis and which resists many chemotherapeutic regimens, a new treatment modality to control local disease and prevent systemic progression is required. Recently, it was shown that some MRTK cells express HER-2 and are sensitive to anti-HER-2 humanized mAb upon antibody-dependent cell-mediated cytotoxicity with interleukin 2 (47). Moreover, it has been shown that tumor formation from human melanoma-initiating cells is inhibited by anti-ABC5 mAb through antibody-dependent cell-mediated cytotoxicity (48).

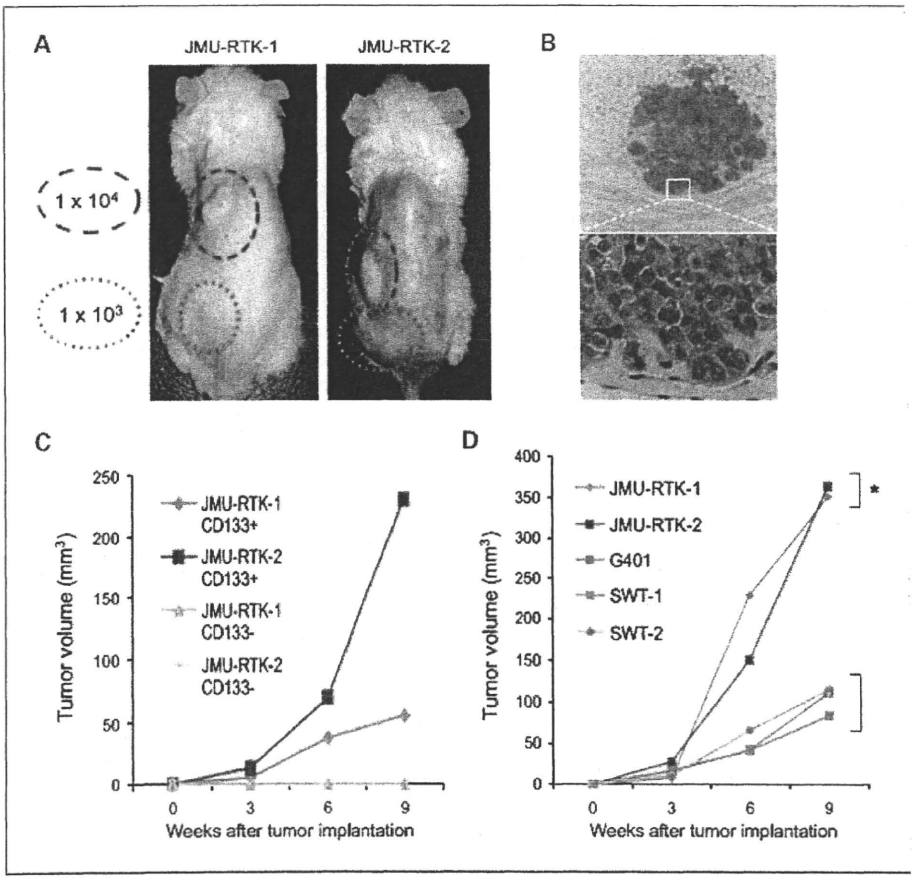

Fig. 4. Tumor growth of $CD133^+$ MRTK enriched cells in NOD/SCID mice. *A*, representative images of JMU-RTK-1 and JMU-RTK-2 tumors at 9 wk following CD133-enriched cell implantation in NOD/SCID mice. CD133-enriched cells (*green dashed*, 1×10^4, and *green dotted*, 1×10^3) were implanted s.c. into the left back of the mice. Notably, CD133-negative cells did not form tumors even with 1×10^5 cells on the right back. *B*, microscopic inspection of CD133-enriched cell implantation (1×10^3 JMU-RTK-1cells). A similar cell morphology is shown in Fig. 1*B*. *C*, JMU-RTK-1 and JMU-RTK-2 cells (1×10^3) following CD133-mediated enrichment were transplanted into the s.c. space of NOD/SCID mice and tumor growth was measured at the indicated time points. *D*, various MRTK cells (1×10^4) following CD133-mediated enrichment in the s.c. space of NOD/SCID mice and tumor growth was measured at the indicated time points. *, $P < 0.05$ (JMU-RTK-1 and JMU-RTK-2, vs G401, SWT-1, and SWT-2), Tukey-Kramer test.

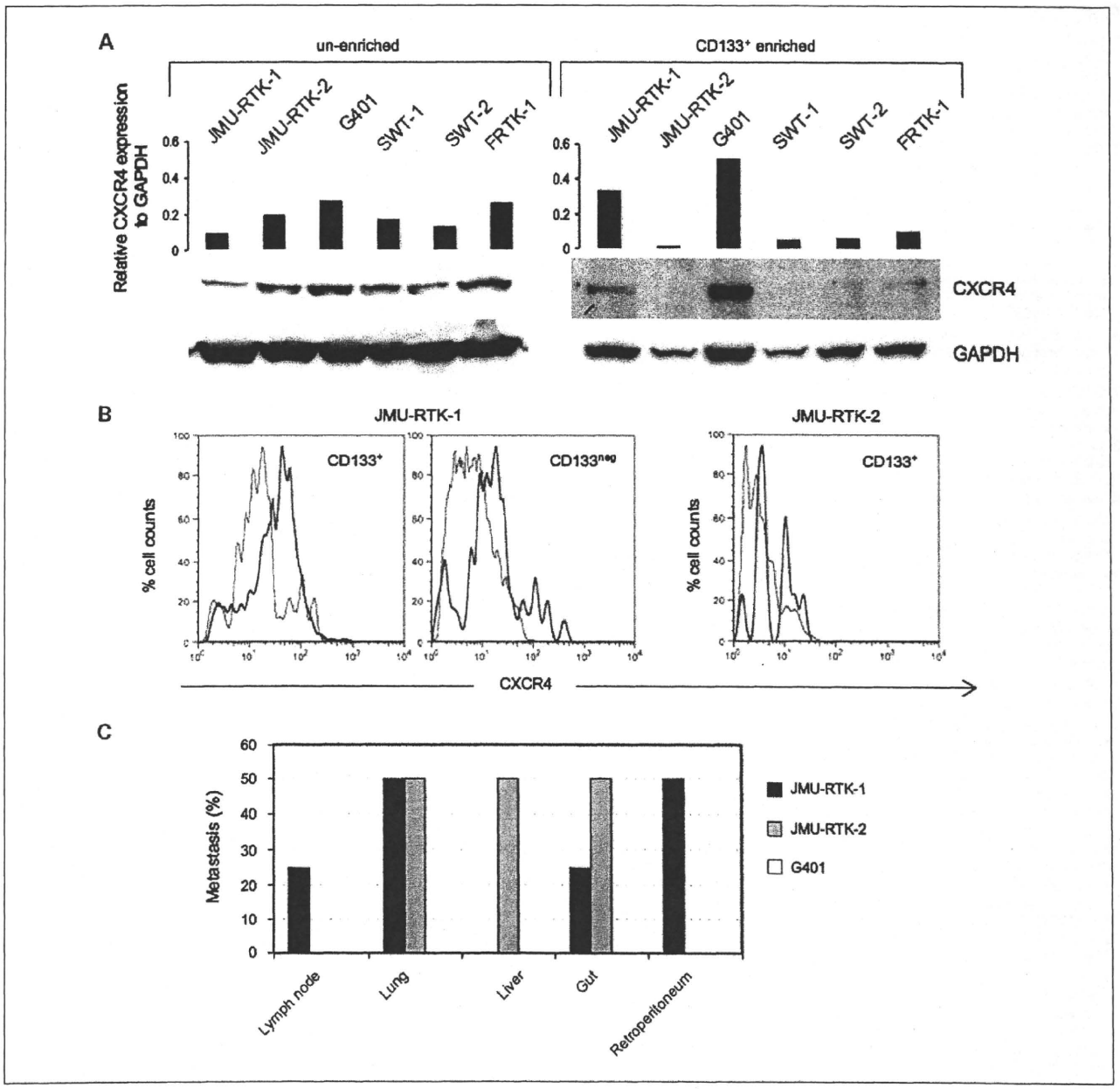

Fig. 5. CXCR4 expression in CD133$^+$-enriched MRTK cells. *A*, Western blot analysis of CXCR4 in MRTK cells. Cells were lysed and analyzed for CXCR4 before and after CD133 enrichment using magnetic bead selection. GAPDH was used as an internal control. One of two independent experiments with similar results. *B*, CXCR4 expression in JMU-RTK-1 and JMU-RTK-2 cells following CD133$^+$ enrichment. CXCR4 expression was analyzed after gating the CD133$^+$ and CD133$^-$ population. Solid line, CXCR4; dashed line, isotype-matched IgG. One of two independent experiments with similar results. *C*, a graph of metastatic frequency of luciferase-expressing MRTK cells following CD133 enrichment. CD133$^+$-enriched cells were transplanted into the left kidney of SCID mice (4-5 mice per cell line). Tumor-derived photons were examined *ex vivo* 30 d following tumor implantation.

Although present therapeutic strategies provide only limited effectiveness against refractory malignancy, the aforementioned evidence suggests that the use of humanized specific antibodies against cancer-initiating cells should provide effective targeting. Although the number of MRTK patients in the present study was very small, our results regarding the identification and characteristics of MRTK-initiating cells provide important implications for the future design of aggressive MRTK therapies.

Disclosure of Potential Conflicts of Interest

No potential conflicts of interest were disclosed.

Acknowledgments

We thank Yasuko Sakuma, Yumi Ohde, and Masayo Kumagai for their skillful technical assistance.

References

1. Reya T, Morrison SJ, Clarke MF, Weissman IL. Stem cells, cancer, and cancer stem cells. Nature 2001;414: 105–11.
2. Beachy PA, Karhadkar SS, Berman DM. Tissue repair and stem cell renewal in carcinogenesis. Nature 2004; 432:324–31.
3. Stingl J, Caldas C. Molecular heterogeneity of breast carcinomas and the cancer stem cell hypothesis. Nat Rev Cancer 2007;7:791–9.
4. Lobo NA, Shimono Y, Qian D, Clarke MF. The biology of cancer stem cells. Annu Rev Cell Dev Biol 2007;23: 675–99.
5. Al-Hajj M, Wicha MS, Benito-Hernandez A, Morrison SJ, Clarke MF. Prospective identification of tumorigenic breast cancer cells. Proc Natl Acad Sci U S A 2003;100:3983–8.
6. Singh SK, Hawkins C, Clarke ID, et al. Identification of human brain tumour initiating cells. Nature 2004;432: 396–401.
7. O'Brien CA, Pollett A, Gallinger S, Dick JE. A human colon cancer cell capable of initiating tumour growth in immunodeficient mice. Nature 2007;445:106–10.
8. Ricci-Vitiani L, Lombardi DG, Pilozzi E, et al. Identification and expansion of human colon-cancer-initiating cells. Nature 2007;445:111–5.
9. Hermann PC, Huber SL, Herrler T, et al. Distinct populations of cancer stem cells determine tumor growth and metastatic activity in human pancreatic cancer. Cell Stem Cell 2007;1:313–23.
10. Collins AT, Berry PA, Hyde C, Stower MJ, Maitland NJ. Prospective identification of tumorigenic prostate cancer stem cells. Cancer Res 2005;65:10946–51.
11. Beckwith J, Palmer N. Histopathology and prognosis of Wilms' tumor: Results of the First National Wilms' Tumor Study. Cancer 1978;41:1937–48.
12. Palmer N, Sutow W. Clinical aspects of the rhabdoid tumor of the kidney. A report of the National Wilms' Tumor Study Group. Med Pediatr Oncol 1983;11:242–5.
13. Versteege I, Sevenet N, Lange J, et al. Truncating mutations of hSNF5/INI1 in aggressive paediatric cancer. Nature 1998;394:203–6.
14. Biegel JA, Zhou JY, Rorke LB, Stenstrom C, Wainwright LM, Fogelgren B. Germ-line and acquired mutations of INI1 in atypical teratoid and rhabdoid tumors. Cancer Res 1999;59:74–9.
15. Tomlinson GE, Breslow NE, Dome J, et al. Rhabdoid tumor of the kidney in the National Wilms' Tumor Study: age at diagnosis as a prognostic factor. J Clin Oncol 2005;23:7641–5.
16. Weeks DA, Beckwith JB, Mierau GW, Luckey DW. Rhabdoid tumor of the kidney. A report of 111 cases from the National Wilms' Tumor Study Pathology Center. Am J Surg Pathol 1989;13:439–58.
17. Murakami T, Maki W, Cardones AR, et al. Expression of CXC chemokine receptor-4 enhances the pulmonary metastatic potential of murine B16 melanoma cells. Cancer Res 2002;62:7328–34.
18. Garvin AJ, Re GG, Tarnowski BI, Hazen-Martin DJ, Sens DA. The G401 cell line, utilized for studies of chromosomal changes in Wilms' tumor, is derived from a rhabdoid tumor of the kidney. Am J Pathol 1993;142: 375–80.
19. Hirose M, Yamada T, Abe T, et al. Establishment and characterization of two cultured cell lines derived from malignant rhabdoid tumors of the kidney. Int J Cancer 1996;67:218–23.
20. Hakozaki M, Hojo H, Sato M, et al. Establishment and characterization of a new cell line, FRTK-1, derived from human malignant rhabdoid tumor of the kidney, with overexpression of epidermal growth factor receptor and cyclooxygenase-2. Oncol Rep 2006;16: 265–71.
21. Sato A, Ohtsuki M, Hata M, Kobayashi E, Murakami T. Antitumor activity of IFN-λ in murine tumor models. J Immunol 2006;176:7686–94.
22. Murakami T, Sato A, Chun NA, et al. Transcriptional modulation using HDACi depsipeptide promotes immune cell-mediated tumor destruction of murine B16 melanoma. J Invest Dermatol 2008; 128:1506–16.
23. Higashino K, Narita T, Taga T, Ohta S, Takeuchi Y. Malignant rhabdoid tumor shows a unique neural differentiation as distinct from neuroblastoma. Cancer Sci 2003;94:37–42.
24. Contag CH, Bachmann MH. Advances in *in vivo* bioluminescence imaging of gene expression. Annu Rev Biomed Eng 2002;4:235–60.
25. Weissleder R, Pittet MJ. Imaging in the era of molecular oncology. Nature 2008;452:580–9.
26. Miraglia S, Godfrey W, Yin AH, et al. A novel five-transmembrane hematopoietic stem cell antigen: isolation, characterization, and molecular cloning. Blood 1997;90:5013–21.
27. Yin AH, Miraglia S, Zanjani ED, et al. AC133, a novel marker for human hematopoietic stem and progenitor cells. Blood 1997;90:5002–12.
28. Suetsugu A, Nagaki M, Aoki H, et al. Characterization of $CD133^+$ hepatocellular carcinoma cells as cancer stem/progenitor cells. Biochem Biophys Res Commun 2006;351:820–4.
29. Yin S, Li J, Hu C, et al. CD133 positive hepatocellular carcinoma cells possess high capacity for tumorigenicity. Int J Cancer 2007;120:1444–50.
30. Eramo A, Lotti F, Sette G, et al. Identification and expansion of the tumorigenic lung cancer stem cell population. Cell Death Differ 2008;15:504–14.
31. Shmelkov SV, Butler JM, Hooper AT, et al. CD133 expression is not restricted to stem cells, and both $CD133^+$ and $CD133^-$ metastatic colon cancer cells initiate tumors. J Clin Invest 2008;118:2111–20.
32. Shmelkov SV, Jun L, St Clair R, et al. Alternative promoters regulate transcription of the gene that encodes stem cell surface protein AC133. Blood 2004; 103:2055–61.
33. Balkwill F. Cancer and the chemokine network. Nat Rev Cancer 2004;4:540–50.
34. Murakami T, Cardones AR, Hwang ST. Chemokine receptor and melanoma metastasis. J Dermatol Sci 2004;36:71–8.
35. Rubin JB, Kung AL, Klein RS, et al. A small-molecule antagonist of CXCR4 inhibits intracranial growth of primary brain tumors. Proc Natl Acad Sci U S A 2003;100:13513–8.
36. Zeelenberg IS, Ruuls-Van Stalle L, Roos E. The chemokine receptor CXCR4 is required for outgrowth of colon carcinoma micrometastases. Cancer Res 2003; 63:3833–9.
37. Koshiba T, Hosotani R, Miyamoto Y, et al. Expression of stromal cell-derived factor 1 and CXCR4 ligand receptor system in pancreatic cancer: a possible role for tumor progression. Clin Cancer Res 2000;6:3530–5.
38. Scala S, Ottaiano A, Ascierto PA, et al. Expression of CXCR4 predicts poor prognosis in patients with malignant melanoma. Clin Cancer Res 2005;11: 1835–41.
39. Kim J, Takeuchi H, Lam ST, et al. Chemokine receptor CXCR4 expression in colorectal cancer patients increases the risk for recurrence and for poor survival. J Clin Oncol 2005;23:2744–53.
40. Xu F, Wang F, Di M, et al. Classification based on the combination of molecular and pathologic predictors is superior to molecular classification on prognosis in colorectal carcinoma. Clin Cancer Res 2007;13: 5082–8.
41. Dalerba P, Clarke MF. Cancer stem cells and tumor metastasis: first steps into uncharted territory. Cell Stem Cell 2007;1:241–2.
42. Balkwill F, Mantovani A. Inflammation and cancer: back to Virchow? Lancet 2001;357:539–45.
43. Coussens LM, Werb Z. Inflammatory cells and cancer: think different! J Exp Med 2001;193:F23–6.
44. Burns JM, Summers BC, Wang Y, et al. A novel chemokine receptor for SDF-1 and I-TAC involved in cell survival, cell adhesion, and tumor development. J Exp Med 2006;203:2201–13.
45. Miao Z, Luker KE, Summers BC, et al. CXCR7 (RDC1) promotes breast and lung tumor growth *in vivo* and is expressed on tumor-associated vasculature. Proc Natl Acad Sci U S A 2007;104:15735–40.
46. Wang J, Shiozawa Y, Wang J, et al. The role of CXCR7/RDC1 as a chemokine receptor for CXCL12/SDF-1 in prostate cancer. J Biol Chem 2008;283: 4283–94.
47. Katsumi Y, Kuwahara Y, Tamura S, et al. Trastuzumab activates allogeneic or autologous antibody-dependent cellular cytotoxicity against malignant rhabdoid tumor cells and interleukin-2 augments the cytotoxicity. Clin Cancer Res 2008;14:1192–9.
48. Schatton T, Murphy GF, Frank NY, et al. Identification of cells initiating human melanomas. Nature 2008;451:345–9.

STEM CELLS
TISSUE-SPECIFIC STEM CELLS

Intra-articular Injected Synovial Stem Cells Differentiate into Meniscal Cells Directly and Promote Meniscal Regeneration Without Mobilization to Distant Organs in Rat Massive Meniscal Defect

MASAFUMI HORIE,[a] ICHIRO SEKIYA,[b] TAKESHI MUNETA,[a,c] SHIZUKO ICHINOSE,[d] KENJI MATSUMOTO,[e] HIROHISA SAITO,[e] TAKASHI MURAKAMI,[f] EIJI KOBAYASHI[f]

[a]Section of Orthopedic Surgery, [b]Section of Cartilage Regeneration, Graduate School, [c]Global Center of Excellence Program and International Research Center for Molecular Science in Tooth and Bone Diseases, and [d]Instrumental Analysis Research Center, Tokyo Medical and Dental University, Tokyo, Japan; [e]Department of Allergy and Immunology, National Research Institute for Child Health and Development, Tokyo, Japan; [f]Division of Organ Replacement Research, Center for Molecular Medicine, Jichi Medical University, Tochigi, Japan

Key Words. Mesenchymal stem cells • Synovium • Meniscus • Luciferase • LacZ • Cell transplantation

ABSTRACT

Osteoarthritis in the knees, which can be caused by meniscal defect, constitutes an increasingly common medical problem. Repair for massive meniscal defect remains a challenge owing to a lack of cell kinetics for the menisci precursors in knee joint. The synovium plays pivotal roles during the natural course of meniscal healing and contains mesenchymal stem cells (MSCs) with high chondrogenic potential. Here, we investigated whether intra-articular injected synovium-MSCs enhanced meniscal regeneration in rat massive meniscal defect. To track the injected cells, we developed transgenic rats expressing dual luciferase (Luc) and LacZ. The cells derived from synovium of the rats demonstrated colony-forming ability and multipotentiality, both characteristics of MSCs. Hierarchical clustering analysis revealed that gene expression of meniscal cells was closer to that of synovium-MSCs than to that of bone marrow-MSCs. Two to 8 weeks after five million Luc/LacZ+ synovium-MSCs were injected into massive meniscectomized knee of wild-type rat, macroscopically, the menisci regenerated much better than it did in the control group. After 12 weeks, the regenerated menisci were LacZ positive, produced type 2 collagen, and showed meniscal features by transmission electron microscopy. In in-vivo luminescence analysis, photons increased in the meniscus-resected knee over a 3-day period, then decreased without detection in all other organs. LacZ gene derived from MSCs could not be detected in other organs except in synovium by real-time PCR. Synovium-MSCs injected into the massive meniscectomized knee adhered to the lesion, differentiated into meniscal cells directly, and promoted meniscal regeneration without mobilization to distant organs. STEM CELLS *2009;27:878–887*

Disclosure of potential conflicts of interest is found at the end of this article.

INTRODUCTION

The meniscus is a wedge-shaped semilunar fibrocartilage that lies between the weight bearing joint surfaces of the femur and the tibia. For symptomatic meniscus injury, a meniscectomy is often performed. This, however, often leads to osteoarthritis [1]. Meniscal suture to preserve its function is limited for its indication, and the result is not always satisfactory due to poor healing of the meniscus. Despite other therapeutic attempts [2], problems related to its effectiveness and invasion persist. A novel strategy for meniscus injury remains necessary.

Mesenchymal stem cells (MSCs) are postulated to participate in tissue homoeostasis, remodeling, and repair by ensuring the replacement of mature cells lost to physiological turnover, senescence, injury, or disease. Stem cell populations are found in most adult tissues, and in general, their differentiation potential may reflect the local cell population. Developmentally, intra-articular tissues are differentiated from common progenitors, referred to as common interzone cells [3]. Synovium-MSCs have high

Author contributions: M.H.: conception and design, data analysis, collection of data, and manuscript writing; I.S.: conception and design, financial support, manuscript writing, final approval of manuscript; T. Muneta: conception and design, financial support, and administrative support; S.I.: electron microscopy; K.M.: microarray and real-time PCR; H.S.: microarray and real-time PCR; T. Murakami: provision of study material and manuscript writing; E.K.: conception and design, financial support, administrative support, provision of study material, manuscript writing.

Correspondence: Ichiro Sekiya, M.D., Ph.D., Section of Cartilage Regeneration, Graduate School, Tokyo Medical and Dental University, 1-5-45 Yushima, Bunkyo-Ku, Tokyo 113-8519, Japan. Telephone: +81-3-5803-4675; Fax: +81-3-5803-0266; e-mail: sekiya.orj@tmd.ac.jp; or Eiji Kobayashi, M.D., Ph.D., Division of Organ Replacement Research, Center for Molecular Medicine, Jichi Medical University, 3311-1 Yakushiji, Shimotsuke, Tochigi 329-0498, Japan. Telephone: +81-285-58-7446; Fax: +81-285-44-5365; e-mail: eijikoba@jichi.ac.jp Received July 16, 2008; accepted for publication December 9, 2008; first published online in STEM CELLS *EXPRESS* January 8, 2009. 1066-5099/2009/$30.00/0 doi: 10.1634/stemcells.2008-0616

chondrogenic potential [4, 5], clinically increase in number in synovial fluid after intra-articular tissue injury to contribute to its repair in part [6] and expand in the presence of pure synovial fluid in tissue cultures of the synovium [7]. Synovial tissue may serve as a reservoir of stem cells that mobilize following injury and migrate to the wound site where, in cooperation with local cells, they participate in the repair response.

Thus, during the natural course of meniscal repair, synovium-MSCs are a potential cell source. Here, we investigated whether intra-articular injected synovium-MSCs enhanced meniscal regeneration in rat massive meniscal defect. Dual colored transgenic (Tg) rats expressing luciferase and LacZ (Luc/LacZ) were created for this study so that the fate of transplanted cells could be traced dynamically and precisely.

Materials and Methods

Establishment of Dual Colored Transgenic Rat

Dual colored Tg rats expressing luciferase and Lac-Z were created by cross-breeding ROSA/luciferase Tg Lewis rats [8] with ROSA/LacZ Lewis rats [9]. The expression of luciferase was detected by an in vivo bioimaging system, and the expression of LacZ was detected by X-gal staining (detailed later). The F1 hybrids between ROSA/luciferase Tg and ROSA/LacZ Lewis rat neonate were imaged after *intraperitoneal injection of* D-luciferin (30 mg/kg per body weight) (potassium salt; Biosynth, Postfach, Switzerland, http://www.biosynth.com), and then they were stained with X-gal. In the same manner, luciferase and LacZ expressions were examined in various tissues of these rats. Approximately one-fourth of these F1 hybrids expressed luciferase and LacZ in the whole body. We used these "dual colored" F1 hybrids expressing both luciferase and LacZ (Luc/LacZ) for the donor of MSCs.

MSCs Preparation

All experiments were conducted in accordance with the institutional guidelines for the care and use of experimental animals of Tokyo Medical and Dental University and Jichi Medical University. The synovial membranes of bilateral knee joints were excised, minced, and digested for 3 hours at 37°C with type V collagenase (0.2%; Sigma-Aldrich, St. Louis, MO, http://www.sigmaaldrich.com), and passed through a 40-μm filter (Becton Dickinson, Franklin Lakes, NJ, http://www.bd.com). Bone marrow was extruded by inserting a 22-gauge needle into the shaft of the femur and tibia bone and flushed out. Synovium and bone marrow cells were cultured in a complete medium (αMEM; Invitrogen, Carlsbad, CA, http://www.invitrogen.com; 20% FBS; Invitrogen; 100 units per milliliter penicillin, 100 μg/ml streptomycin, and 2 mM L-glutamine; Invitrogen) for 14 days. Then the cells were replated at 100 cells/cm^2, cultured for 14 days, and frozen at −80°C as passage 1. The stocked cells were rapidly thawed in a water bath at 37°C, plated in a 150 cm^2 dish, and harvested after 5 days. Then the cells were replated at 100 cells/cm^2, cultured for 14 days, and collected for further analyses [5]. For colony-forming assay, 100 cells were plated in 60 cm^2 dishes and cultured for 14 days. The dishes were stained with X-gal, and the same dishes were then stained with 0.5% Crystal Violet.

In Vitro Differentiation Assay

For adipogenesis, the cells were cultured in the adipogenic medium that consisted of a complete medium supplemented with 0.5 μM dexamethasone, 0.5 mM isobutylmethylxanthine, and 50 μM indomethacin. After 4 days, the adipogenic cultures were stained with 0.3% Oil Red-O solution or X-gal solution [10].

For osteogenesis, the cells were cultured in the calcification medium in the presence of 100 nM dexamethasone, 10 mM β-glycerophosphate, and 50 μM ascorbic acid. After an additional 6 weeks, the dishes were stained with 0.5% Alizarin Red solution or X-gal solution.

For in vitro chondrogenesis, 8×10^5 cells were placed in a 15 ml polypropylene tube (BD Falcon, Bedford, MA, http://www.bdbiosciences.com) and pelleted by centrifugation at 450g for 10 minutes. The pellets were cultured for 21 days in chondrogenic media, which contained 500 ng/ml BMP-2 (Astellas Pharma Inc., Tokyo, Japan, http://www.astellas.com), in addition to high-glucose Dulbecco's modified Eagle's medium (Invitrogen) supplemented with 10 ng/ml transforming growth factor-β3 (TGF-β3) (R&D Systems Inc., Minneapolis, MN, http://www.rndsystems.com), 10^{-7} M dexamethasone, 50 μg/ml ascorbate-2-phosphate, 40 μg/ml proline, 100 μg/ml pyruvate, and 50 mg/ml ITS+TMPremix (Becton Dickinson). For histological analysis, the pellets were embedded in paraffin, cut into 5-μm sections, and stained with 1% Toluidine Blue [11].

Flow Cytometry

Synovium-MSCs at passage 3 were harvested 14 days after plating. One million cells were suspended in 500 μl phosphate buffered saline (PBS) containing 20 ng/ml fluorescein isothiocyanate (FITC) or phycoerythrin (PE)-coupled antibodies against CD11b, CD45, CD90 (Becton Dickinson), CD34 (Santa Cruz Biotechnology Inc., Santa Cruz, CA, http://www.scbt.com), and CD29 (BioLegend, San Diego, CA, http://www.biolegend.com) As an isotype control, FITC- or PE-coupled nonspecific mouse IgG (Becton Dickinson) was substituted for the primary antibody. After incubation for 30 minutes at 4°C, the cells were washed with PBS and resuspended in 1 ml PBS for analysis. Cell fluorescence was evaluated by flow cytometry in a FACSCalibur instrument (Becton Dickinson); data were analyzed by using CellQuest software (Becton Dickinson).

Oligonucleotide Microarray

For rat meniscal cells, menisci were minced, digested for 3 hours at 37°C with type II collagenase (0.2%; Sigma), and passed through a 40 μm filter (Becton Dickinson). Nucleated cells were plated at 100 cells/cm^2 and cultured in a complete medium. Total RNA was isolated from passage 1 colony-formed cells derived from the synovium, bone marrow [5], and meniscus with the RNeasy Total RNA Mini Kit (Qiagen, Valencia, CA, http://www1.qiagen.com).

A comprehensive microarray analysis was performed using 3 μg of total RNA from each sample and GeneChip Rat 230 2.0 probe arrays (Affymetrix, Santa Clara, CA, http://www.affymetrix.com) [12]. Data analysis was performed with GeneSpring software version 7.2 (Agilent Technologies, Palo Alto, CA, http://www.agilent.com). To normalize the variations in staining intensity among chips, the "Signal" values for all genes on a given chip were divided by the median value for the expression of all genes on the chip. To eliminate genes containing only a background signal, genes were selected only if the raw values of the "Signal" were more than 30, and expression of the gene was judged to be "Present" by the GeneChip Operating Software version 1.4 (Affymetrix). After elimination, expression data of a total of 14,882 probe sets were employed for further analysis. A hierarchical-clustering analysis was performed using a minimum distance value of 0.001, a separation ratio of 0.5, and the standard definition of the correlation distance. A dendrogram was obtained from a hierarchically clustering analysis using average linkage and distance metric equal to one minus the Pearson correlation applied to the microarray data [13].

Meniscectomy and MSCs Injection

Wild-type male Lewis rats at 12 weeks of age (Charles River, Yokohama, Japan, http://www.crj.co.jp) were used (n = 27). Under anesthesia, a straight incision was made on the anterior side of bilateral knee, the anteromedial side of the joint capsule was cut, and the anterior horn of the medial meniscus was dislocated anteriorly with a forceps. The meniscus was then cut vertically at the level of medial collateral ligament, and the anterior half of medial meniscus was excised. The dislocated meniscus was removed and the wound was closed in layers. Immediately after the skin incision was closed, a 27-gauge needle was inserted

at the center of the triangle formed by the medial side of the patellar ligament, the medial femoral condyle, and the medial tibial condyle, toward the intercondylar space of the femur. Then 5 × 10^6 Luc/LacZ$^+$ synovium-MSCs (n = 14) or bone marrow-MSCs (n = 9) in 50 μl PBS were injected into the right knee joint. For the control, the same volume of PBS was injected into the left knee. The rats were allowed to walk freely in the cage.

For control of in vivo Imaging analysis, 5 × 10^6 Luc/LacZ$^+$ synovium-MSCs were injected into the normal right knee of the wild-type Lewis rats (n = 4).

Histology and Detection of LacZ Expression

The whole medial meniscus was collected at 2, 4, 8, and 12 weeks after MSCs injection (n = 3 each time point). The samples were fixed with a fixative solution (0.2% glutaraldehyde, 2 mM $MgCl_2$, and 5 mM EGTA) in PBS for 10-30 minutes at room temperature and washed three times in a washing solution (2 mM $MgCl_2$, 0.01% sodium deoxycholate, and 0.02% Nonidet P40) in PBS. Then they were treated with an X-gal staining solution (1 mg/ml of 5-bromo-4-chloro-3-indolyl-β-D-galactopyranoside, 2 mM $MgCl_2$, and 5 mM potassium hexacyanoferrate [III], 5 mM potassium hexacyanoferrate [II] trihydrate) at 37°C for 3 hours. They were subsequently fixed again in 4% paraformaldehyde and decalcified with 0.5 M EDTA (pH 7.5) for 3 days at 4°C, followed by a gradient replacement with 20% sucrose for 24 hours at 4°C, and then evaluated by Toluidine Blue or Eosin staining of paraffin sections.

Immunostaining

Sections were pretreated with 0.4 mg/ml proteinase K (DAKO, Carpinteria, CA, http://www.dakousa.com) in Tris-HCl for 15 minutes at room temperature for optimal antigen retrieval. Residual enzymatic activity was removed by washes in PBS, and nonspecific staining was blocked with PBS containing 10% normal horse serum for 20 minutes at room temperature. A primary anti-rat monoclonal antibody against human type II collagen (1 : 200 dilution with PBS containing 1% BSA; Daiichi Fine Chemical, Toyama, Japan, http://www.daiichi-fcj.co.jp) was applied to the section which was incubated at room temperature for 1 hour and rinsed again with PBS. Immunostaining was detected by Vectastain ABC reagent (Vector Laboratories, Burlingame, CA; http://www.vectorlabs.com), followed by diaminobenzidine staining.

In Vivo Bioluminescent Imaging

A noninvasive bioimaging system IVIS (Xenogen, Alameda, CA, http://www.caliperls.com) was used for analysis using IGOR (WaveMetrics, Lake Oswego, OR, http://www.wavemetrics.com) and IVIS Living Image (Xenoxgen) software packages [14]. To detect photons from Luc$^+$ cells, undifferentiated MSCs or chondrocyte pellets were suspended in PBS and imaged immediately after the addition of 0.15 mg D-luciferin (potassium salt; Biosynth). Also, for transplanted cell tracking in vivo, D-luciferin was injected into the penile vein of anesthetized rats (30 mg/kg per body weight) under anesthesia with isoflurane. The signal intensity was quantified as photon flux in units of photons per seconds cm^2 per steradian in the region of interest.

Transmission Electron Microscopy

The regenerated tissues at 12 weeks in the synovium-MSCs treated group and control groups were selected and fixed with 2.5% glutaraldehyde in 0.1 M PBS for 5 hours, washed overnight at 4°C in the same buffer, postfixed with 1% OsO_4 buffered with 0.1 M PBS for 2 hours, dehydrated in a graded series of ethanol, and embedded in Epon 812. Ultrathin sections at 90 nm were collected on copper grids, double-stained with uranyl acetate and lead citrate, and then examined with a transmission electron microscope (H-7100, Hitachi, Hitachinaka, Japan, http://www.hitachi.co.jp) [15].

Quantitative Real-Time PCR

Total RNAs were prepared from brain, lung, liver, spleen, kidney, and knee synovium at 3 days after the synovium-MSCs injected rat by RNAqueous Kit (Ambion, ***Austin, TX;*** http://www.ambion.com) according to the manufacturer's instructions. For the positive control, total RNAs from various organs of Luc/LacZ Tg rat and expanded MSCs including Luc/LacZ positive cell rates ranged from 0.001 to 100% were used. Also total RNAs from various organs of wild-type rat were prepared as a negative control. They were subjected to *real-time PCR* to measure the level of LacZ.

The primer sets for LacZ, (sense, 5′-GGTGCAGAGAGACAGGAACCAC-3′; antisense, 5′-CCTTCATACTGCACAGGTCTGCT-3′) and β-actin (sense, 5′-CCGAGCGTGGCTACAGCTT-3′; antisense, 5′-GGCAGTGGCCATCTCTTGC-3′) were synthesized at FASMAC (Kanagawa, Japan, http://www.fasmac.co.jp).

First-strand cDNA was synthesized using the I Script cDNA synthesis kit (Bio-Rad Laboratories, Hercules, CA, http://www.bio-rad.com) with an Oligo (dT) (12-18mers) primer. Real-time quantitative PCR analyses were performed with the ABI Prism 7700 Sequence Detection System (Applied Biosystems, Foster City, CA, http://www.appliedbiosystems.com) using SYBR Green I PCR reagents (TOYOBO, Osaka, Japan, http://www.toyobo.co.jp/e/) as described previously [12]. To determine the exact copy numbers of the target genes, the quantified concentrations of subcloned PCR fragments of LacZ and β-actin were serially diluted and used as standards in each experiment. Aliquots of cDNA equivalent to 5 ng of total RNA samples were used for each real-time PCR. Data were normalized with β-actin levels in each sample. The copy number is expressed as the number of transcripts per nanogram total RNA.

Statistics

The Mann-Whitney U test was used to compare two groups at each period. p values less than .05 were considered significant.

Results

Synovium-MSCs Expressing Luc/LacZ Genes

The F1 hybrids between ROSA/luciferase Tg and ROSA/LacZ Lewis rat neonate produced luminescence after intraperitoneal injection of D-luciferin (Fig. 1A), and then they were positive for X-gal staining (Fig. 1B). In the same manner, we next examined luciferase and LacZ expression in various tissues of these rats. Approximately one-fourth of these F1 hybrids expressed luciferase and LacZ in whole body including the synovium (Fig. 1C). We termed these "dual colored" rats as Luc/LacZ Tg rats. MSCs were isolated from the synovium of Luc/LacZ Tg rats. In vitro imaging of luciferase activity showed that as few as one thousand MSCs were detected over the background in the linear dose-dependent output of luminescence (Fig. 1D, 1E). Synovium-MSCs from Luc/LacZ Tg rats formed LacZ$^+$ single cell-derived colonies consisting of spindle cells (Fig. 1F). They could differentiate into adipocytes (Fig. 1G) and calcified with LacZ expression in vitro (Fig. 1H). The cells could also form cartilage with expressions of both LacZ and luciferase (Fig. 1I). The cells derived from synovium of Luc/LacZ Tg rat demonstrated characteristics of MSCs, and the dual markers were maintained after the differentiation. Flow cytometric analysis demonstrated that the majority of synovium-MSCs expressed CD29 and CD90, and were negative for CD11b, CD34, and CD45 (Fig. 1J).

Hierarchical clustering analysis revealed that the gene expression of meniscal cells was closer to that of synovium-MSCs than that of bone marrow-MSCs (Fig. 2). This indicates that synovium-MSCs may retain a more advantageous character as a MSC source for meniscal regeneration than bone marrow-MSCs.

Meniscal Regeneration After Intra-articular Injection of Synovium-MSCs

To obtain in vivo evidence to support the synovium-MSCs potential, we performed massive meniscectomy in both sides

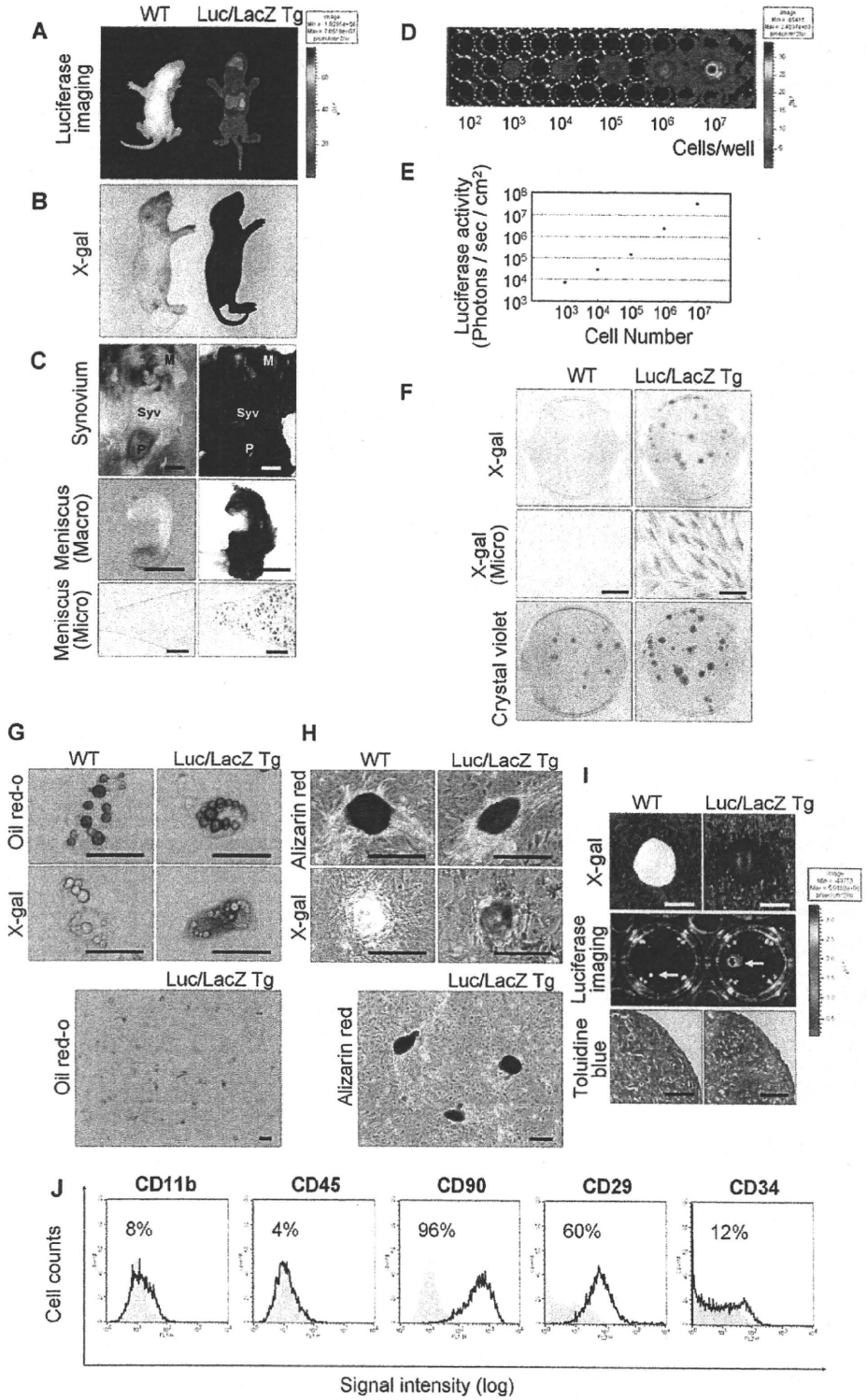

Figure 1. Mesenchymal stem cells (MSCs) derived from the synovium of Luc/LacZ transgenic (Tg) rats expressing dual reporter genes. **(A):** Luminescent images of wild and Luc/LacZ Tg rats. **(B):** Wild and Luc/LacZ Tg rats stained with X-gal. **(C):** Knee synovium and meniscus of wild and Luc/LacZ Tg rats stained with X-gal. Scale bar in upper and middle: 2 mm. Scale bar in lower: 100 μm. **(D):** Bioluminescent imaging of varying numbers of synovium-MSCs from Luc/LacZ Tg rats. **(E):** Quantification for bioluminescent imaging of varying numbers of synovium-MSCs. **(F):** Colony forming ability of MSCs from Luc/LacZ Tg rat synovium. X-gal positive colony forming cells 14 days after the plating of 100 cells in 60 cm^2 dishes (top). Microscopic appearances of X-gal positive spindle cells (middle). Scale bars: 50 μm. Total colonies in the same dishes stained with crystal violet (bottom). **(G):** Adipogenesis. Scale bars: 25 μm. **(H):** Calcification. Scale bars: 100 μm. **(I):** Chondrogenesis. Cartilage pellets stained with X-gal (top). Scale bars: 500 μm. Bioluminescent imaging of cartilage pellets (middle). Histological section stained with toluidine blue (bottom). Scale bar = 100 μm. **(J):** Flow cytometric analysis of synovium-MSCs at passage 3. CD11b, CD45, CD90, CD29, and CD 34 expression are shown as an open plot and isotype control expression as a shaded plot. Abbreviations: M, meniscus; P, patella; Syv, synovium; WT, wild-type.

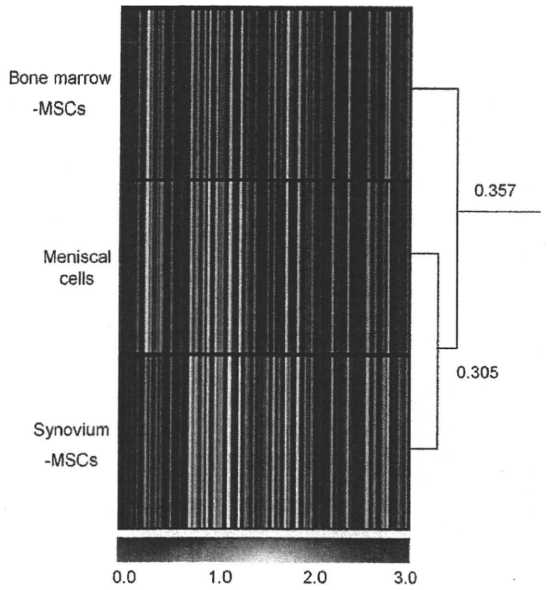

Figure 2. Dendrogram resulting from a hierarchically clustering analysis for gene profile of rat bone marrow-MSCs, synovium-MSCs, and meniscal cells. Gene expression was analyzed with the GeneChip Rat 230 2.0 probe arrays. Data of 14,882 probe sets were analyzed by applying a hierarchical tree algorithm to the normalized intensity. The color code for the signal strength in the classification scheme is shown in the box below. High-expression genes are indicated by shades of red and low expression genes are indicated by shades of blue. The dendrogram at the right provides a measure of the relatedness of gene expression profile in each sample (one minus the Pearson correlation). Abbreviation: MSCs, mesenchymal stem cells.

of the knee of wild rats (Fig. 3A), and Luc/LacZ^{+} synovium-MSCs suspension (5×10^6 in 50 μl PBS) were injected into the right knee joint immediately after the incision was closed. For the control, the same volume of PBS was injected into the left knee. At 2 weeks, dark blue areas for LacZ were observed around the meniscal defect (Fig. 3B, yellow arrow) and sutured capsule (black arrow), indicating that injected synovium-MSCs intensively adhered to injured sites. Dark blue areas for LacZ were still observed around the meniscal defect and sutured capsule, but not observed in intact synovium, cartilage surface, or cruciate ligaments even at 12 weeks (data not shown). At 4 weeks, the anterior part of the meniscal defect of MSC injection side exhibited better regeneration than the control side (Fig. 3C).

All menisci for the experiment of synovium-MSCs are shown in Figure 3D. At 2 weeks, the regenerated part of the menisci appeared blue after X-gal staining in the MSC injection group, indicating that injected synovium-MSCs contributed to the repair. Square measures of the meniscus in synovium-MSCs injection groups were significantly larger than those in the control groups at 2, 4, and 8 weeks (Fig. 3E). We also evaluated cartilage and observed fibrillation, ones of the degenerative changes on the surface of the medial femoral condyle and medial tibial plateau in the control group at 12 weeks (Fig. 3F).

When we injected the same amount of bone marrow-MSCs, the meniscal defect was more rapidly regenerated than that on the control side at 4 weeks (Fig. 3D). Macroscopically, there were no remarkable differences between the synovium-MSC injection group and the bone marrow-MSC injection group.

Histologically, the contour of the regenerated menisci sharpened and the ultimate forms were closer to the normal meniscal shape (Fig. 4A). Expression of type II collagen increased in a time-dependent manner. LacZ^{+} MSCs still existed at 12 weeks. In the control group at 12 weeks, regenerated tissue was occupied with less metachromasia, and type II collagen expression was hardly detected. In the bone marrow-MSC injection group, we observed similar features as seen in the synovium-MSC injection group (Fig. 4B).

Electron microscopic analysis of the regenerated meniscus 12 weeks after synovium-MSCs injection demonstrated that round cells with short processes were surrounded by a pericellular matrix, suggesting that meniscal cells were morphologically equivalent to those of the normal meniscus. In contrast, the cell feature in control groups remained to be fibroblastic (Fig. 4C).

Injected MSCs Stay in Knee Joint

The distribution of topically injected synovium-MSCs was evaluated using luciferase-based in vivo imaging. When MSCs were injected into the normal knee ($n = 4$), MSC-derived photons were detected around the right knee, to then decrease within 14 days. When injected into menisectomized knee ($n = 7$), the photons increased in 3 days, then moderately decreased, but could be still observed for 28 days. Substantial luminescence light could not be detected in any other organs of either group (Fig. 5A). Sequential quantification demonstrated that luciferase activities were significantly higher in the meniscectomy group than those in the control group at each time point up to 21 days (Fig. 5B).

To further evaluate whether injected MSCs could migrate to distant organs or not, quantitative real-time PCR was performed. Total RNAs were isolated from the brain, lung, liver, spleen, kidney, and knee synovium of meniscectomized rat at 3 days after the synovium-MSC injection, and were subjected to *real-time PCR* to measure the level of LacZ expression. Injected MSC-derived LacZ gene could be detected only at the injected knee synovium and was not detected in any other organs (Fig. 6). These data confirm the in vivo imaging results and indicate that knee-injected MSCs stayed only in the knee joint.

Discussion

A number of reports have previously described the injection of bone marrow-MSCs into the joint for meniscus injury; however, the kinetics and role of injected MSCs remain unknown. In a goat study, a previously removed medial meniscus regenerated 6 months after MSC injection [16]. However, Caplan et al. suggested in their review article that there were too few prelabeled cells to account for the massive regeneration of the meniscus and inferred that the MSCs trophically enhanced the regeneration of the meniscus [17]. In two other articles, cartilage matrix was present around injected bone marrow MSCs in only a small portion of the injured meniscus, but the roles of injected MSCs were not fully demonstrated [18, 19] To refine our analysis, we created Tg rats expressing dual Luc/LacZ genes.

There are three main factors involved in the interaction between injected synovium-MSCs and meniscal defect: (a) an increase and decrease in the number of the cells, (b) an adherence to the meniscal defect, and (c) differentiation and maintenance.

In in vivo imaging analysis, synovium-MSCs injected into the menisectomized knee transiently increased in number unlike the situation in which the same population of the cells was injected into the intact knee. This indicates that meniscus injury or incision of the articular capsule can produce some cytokines/chemokines to proliferate synovium-MSCs. In a rabbit model,

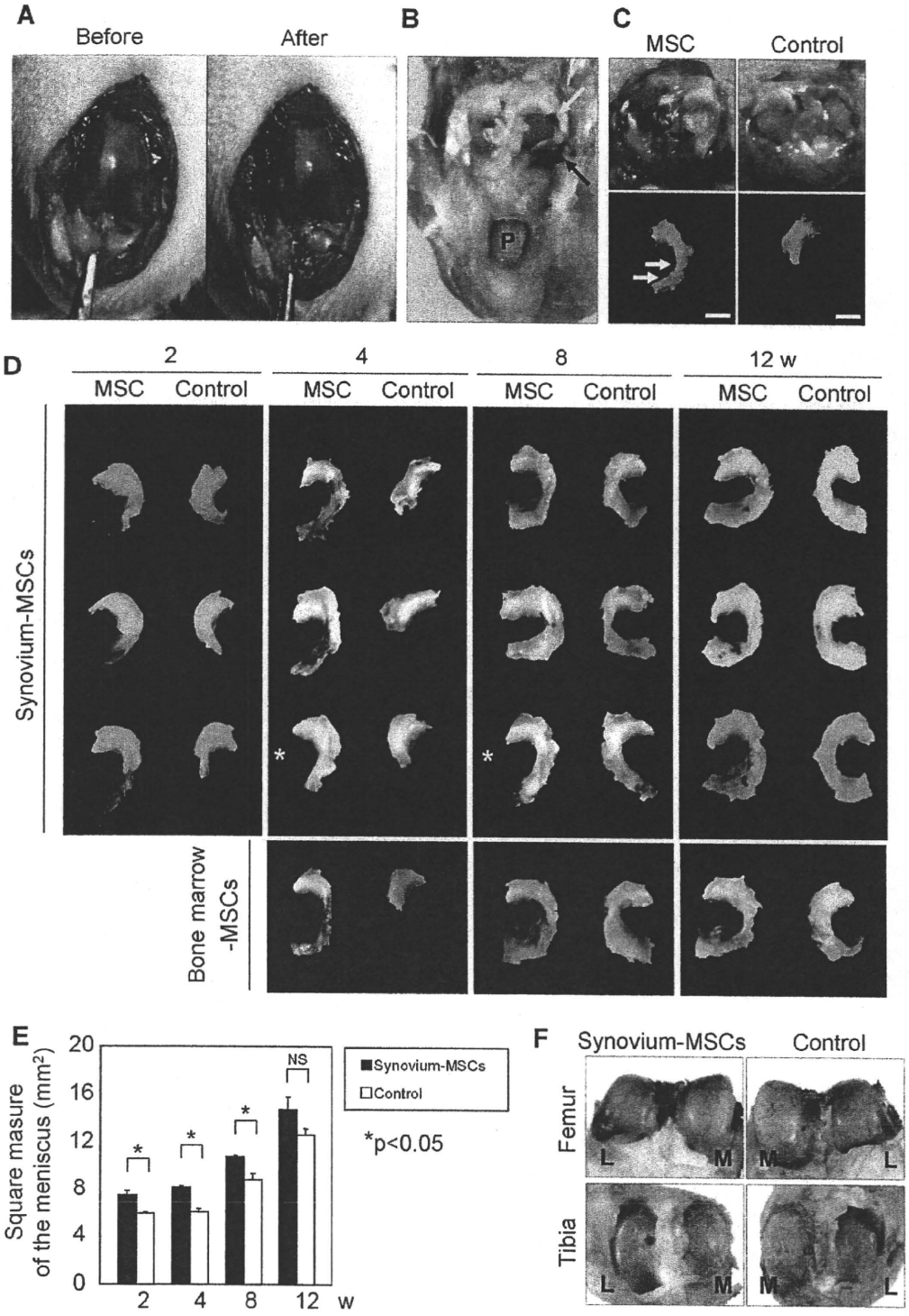

Figure 3. Macroscopic observation of meniscal regeneration after intra-articular injection of synovium-MSCs derived from Luc/LacZ transgenic (Tg) rats. **(A):** Surgical procedure for massive meniscectomy of a wild rat. The medial meniscus was dislocated anteriorly (left, arrowheads), the anterior half of the meniscus was excised, and tibial cartilage was exposed (right, arrow). **(B):** Macroscopic findings of the meniscectomized knee 2 weeks after the injection of synovium MSCs. The knee was stained with X-gal. LacZ positive areas were revealed around the meniscal defect (yellow) and sutured capsule (black). **(C):** Representative macroscopic findings of the tibial joint 4 weeks after synovium-MSCs injection. In the MSC injection group (left), the anterior part of meniscal defect has regenerated (arrow), whereas in the control group, the meniscal defect remains unchanged. Scale bar: 2 mm. **(D):** Macroscopic findings of the regenerated meniscus at 2, 4, 8, and 12 weeks. All menisci were stained with X-gal except those denoted by an asterisk. Representative macroscopic observation of meniscal regeneration after intra-articular injection of bone marrow-MSCs derived from Luc/LacZ Tg rats are shown in the lower part. **(E):** Sequential quantification for area of the meniscus. Values are averages with standard deviations ($n = 3$ for each group). *$p < .05$ between the synovium-MSC group and the control group at each period by Mann-Whitney U test. **(F):** Representative macroscopic findings of the joint surface of femur and tibia 12 weeks after the synovium-MSC group and the control group. The cartilage was stained with India ink. Abbreviations: L, lateral; M, medial; MSCs, mesenchymal stem cells; NS, not significant; P, patella.

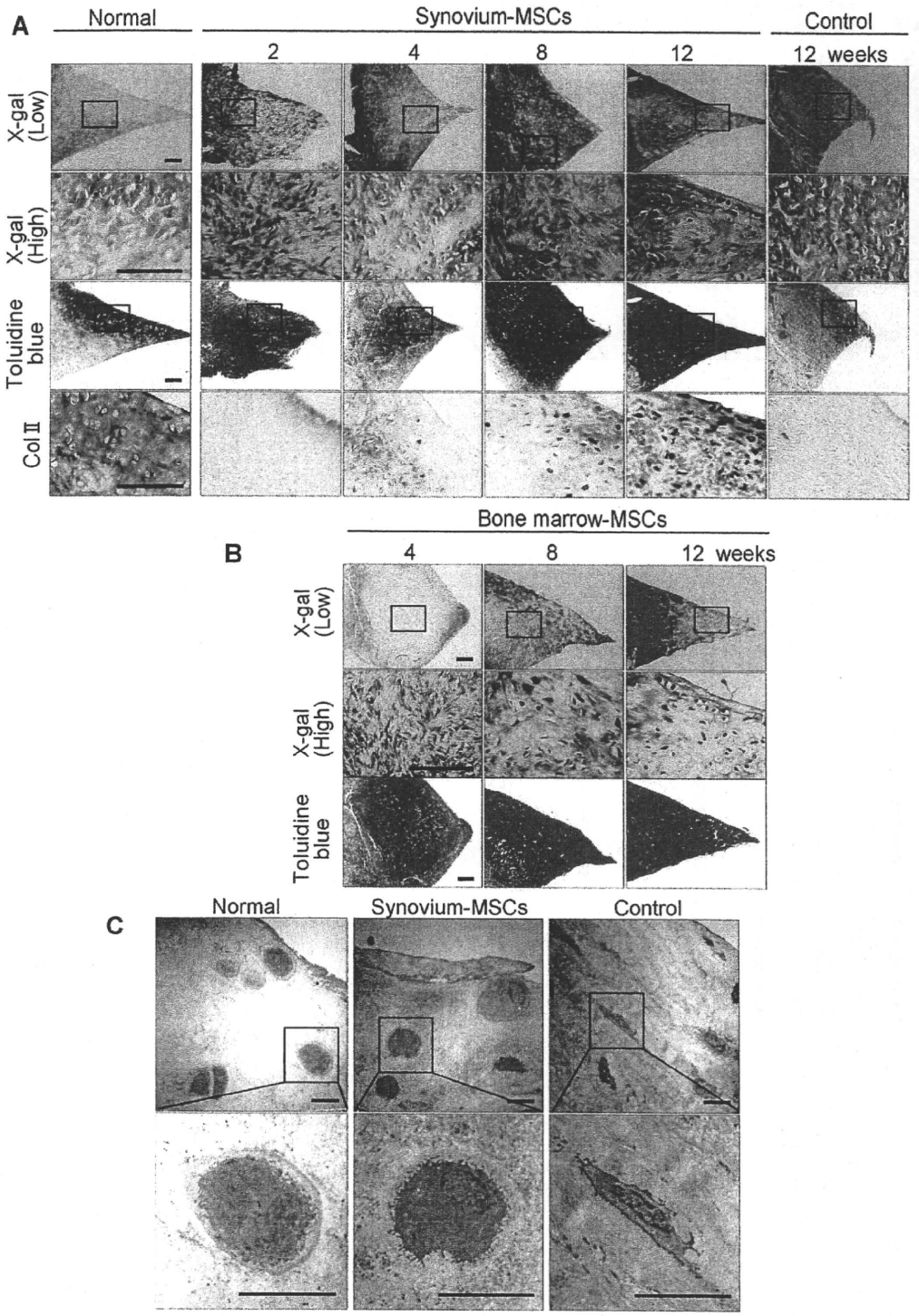

Figure 4. Histological observation of meniscal regeneration after the intra-articular injection of MSCs derived from Luc/LacZ transgenic rats. **(A):** Representative sections of normal meniscus and regenerated tissues in the synovium-MSC injection group stained with X-gal (and eosin as counter staining), toluidine blue, and immunostained with collagen type 2. Scale bar = 100 μm. **(B):** Representative sections of regenerated tissues in the bone marrow-MSC injection group stained with X-gal (and eosin as counter staining), toluidine blue. Scale bar: 100 μm. **(C):** Transmission electron microscopy imaging of typical cells in normal meniscus, regenerated part of meniscus both in the synovium-MSC injection group, and the control group at 12 weeks. Scale bar = 10 μm. Abbreviation: MSCs, mesenchymal stem cells.

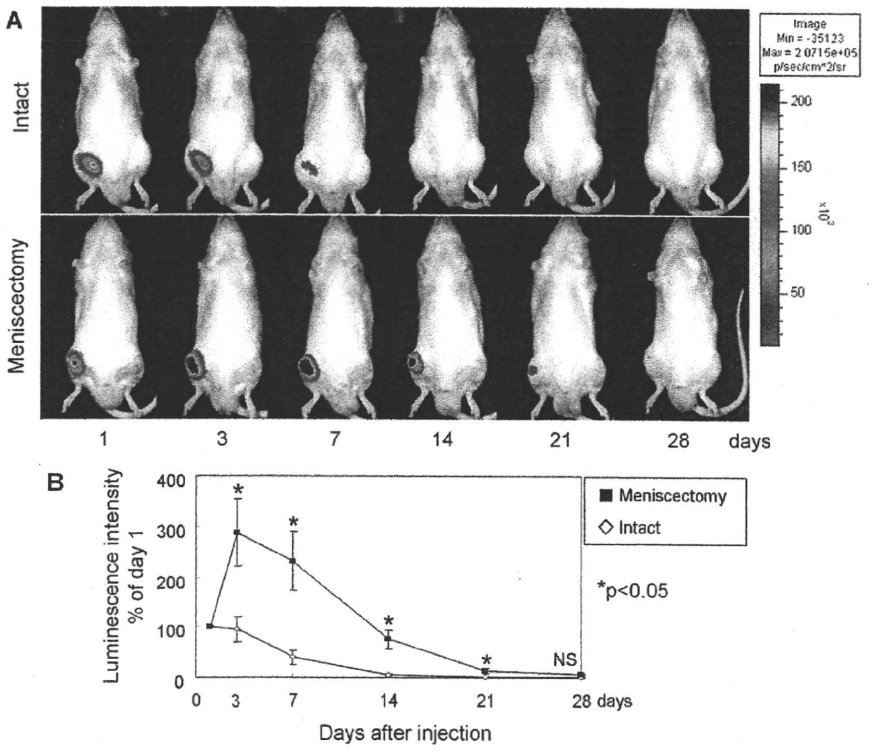

Figure 5. In vivo imaging analysis. **(A):** Imaging of photons from Luc+ cells. Five million synovium-mesenchymal stem cells (MSCs) derived from Luc/LacZ transgenic rats were injected into the intact knee or the meniscectomized knee. Luciferin was injected into the penile vein at indicated points to monitor luminescence driven by synovium-MSCs. **(B):** Sequential quantification of luminescence intensity. Average percentages of the value at 1 day are shown with standard deviations. $*p < .05$ between menisectomy group ($n = 7$) and intact group ($n = 4$) at each period by Mann-Whitney U test. Abbreviations: Max, maximum; Min, minimum; NS, not significant.

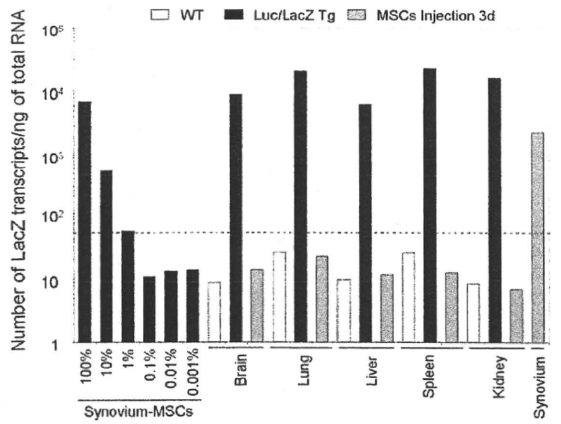

Figure 6. Real-time PCR analysis. The mRNA levels of LacZ obtained from expanded synovium-MSCs and various organs (brain, lung, liver, spleen, kidney, and knee synovium) were determined by SYBR green-based real-time quantitative RT-PCR. The copy number is expressed as the number of transcripts per nanogram of total RNA. The dashed line shows the minimum detection limit (50 copies per nanogram) which was determined by these dilution series. Abbreviations: MSCs, mesenchymal stem cells; Tg, transgenic; WT, wild-type.

meniscal lesions expressed TGF-β, interleukin-1α, and platelet derived growth factor (PDGF) [20]. Human synovium-MSCs have PDGF receptor α and β, and neutralizing PDGF decreases the proliferation of synovium-MSCs in vitro [21]. PDGF may affect the number of transplanted synovium-MSCs.

We could detect MSC-derived photons in the knee joint up to 28 days after the injection but we could not detect it at a longer time point. We have two speculations about this result. One is that a luciferase-based in vivo imaging system cannot detect a small number of Luc^+ cells, as shown in Figure 1D. More than 1,000 cells are needed to detect the light emission. The other is due to blood circulation. The photons are produced only when luciferase is exposed to luciferin substrate and we injected luciferin intravenously. If the Luc^+ cells had existed in the hypovascular area, they could not have been detected. However, in vivo imaging analysis has a great advantage in tracking cells in vivo because we did not have to sacrifice animals, and we could observe the same recipient throughout the observation periods.

Those synovium-MSCs which seem unnecessary for meniscal repair decreased in number and finally fell below measurable limits based on an in vivo imaging system. Possibly, synovium-MSCs participate in intra-articular tissue homoeostasis and repair as do MSCs in mesenchymal tissues throughout the body. This phenomenon differs markedly from ES cells, which form teratomas in the mouse knee joint and subsequently destroy the joint [22]. Induced pluripotent stem cells may hold attraction for future applications, but teratoma formation cannot be overlooked [23].

In vivo imaging analysis suggests that the injected cells did not mobilize out of the injected joint. To confirm this result, we performed real-timePCR to detect Lac Z transcripts. We determined that LacZ transcripts were not detected in brain, lung, liver, spleen, or kidney 3 days after the injection, although the minimum detection limit was 50 copies per nanogram RNA which corresponded to 1% $LacZ^+$ cells. Detection of $LacZ^+$ cells in all sections thorough whole tissues will provide data from another point of view; however, it will be very arduous work.

Injected synovium-MSCs intensively adhered to injured sites of meniscus and synovium. We previously reported that injected synovium-MSCs efficiently adhered to the defect of

articular cartilage [24] and anterior cruciate ligament [6]. The mechanisms that guide the homing of injected cells are not well-understood, but stromal cell-derived factor-1 and monocyte chemotactic protein-1 are candidates to explain them [17].

Undifferentiated synovium-MSCs, attached around the meniscal defect, differentiate into meniscal cells. The environment of the meniscal defect is surrounded by femur and tibia cartilage, synovial tissue, the remaining meniscus, and synovial fluid. The space is also influenced by mechanical stress. This environment itself will provide sufficient signals to induce and maintain meniscal differentiation of synovium-MSCs. Similarly, undifferentiated synovium-MSCs implanted onto an articular cartilage defect differentiate into cartilage cells [25].

In our massive meniscectomized model, bone marrow-MSCs also promoted meniscus regeneration. There were no notable differences of regenerated meniscus in morphology between the synovium-MSC group and the bone marrow-MSC group, although gene profile of synovium-MSCs is closer to that of meniscal cells than that of bone marrow-MSCs. The situation seems to be similar in chondrogenesis as was the case in our previous studies. The gene profile of synovium-MSCs is closer to that of chondrocytes than that of bone marrow-MSCs [26], transplanted bone marrow-MSCs onto the cartilage defect differentiated into chondrocytes at a similar level to that synovium-MSCs which were transplanted in the same way [27]. In contrast, in vivo chondrogenic assay demonstrated that synovium-MSCs produced more cartilage matrix than bone marrow-MSCs [4, 5]. An in vivo model with more sensitivity may distinguish the difference.

Although reparative potential of synovium- and bone marrow-MSCs is similar, synovium-MSCs have an advantage in that they have a higher proliferation potential. In rats, the colony number per nucleated cell was approximately 1/100 in synovium, whereas it was $4/10^5$ in bone marrow. Rat synovium-MSCs expanded much faster than bone marrow-MSCs [5]. Also, human synovium-MSCs proliferated much faster than bone marrow-MSCs when cultured with autologous human serum [21].

For adipogenesis, it usually takes 3 weeks for human bone marrow MSCs to differentiate into adipocytes [10]. In this study, rat bone marrow- and synovium-MSCs differentiated into adipocytes in only 4 days, which was similar to our previous report [5]. Although the content of the adipogenic differentiation medium is similar, the duration to induce sufficient accumulation of lipid vesicles is totally different between MSCs in humans and rats. This indicates the species specificity of MSCs.

For calcification, we found that rat MSCs already calcified in 3 weeks, which was similar to our previous report [5]. In this study, we expected that the calcified area would increase after an additional 3 weeks; therefore, we observed calcification for a total of 6 weeks. Seemingly, the calcified area did not increase during the last 3 weeks (data not shown).

We previously created a 1 mm diameter cylindrical defect in the anterior part of medial meniscus in rats to examine the effect of synovium-MSCs injected intra-articularly. Contrary to our expectation, the cylindrical defect was filled spontaneously, and there was no effect on injected synovium-MSCs through 2-12 weeks [28]. To avoid spontaneous healing, we resected the anterior half of medial meniscus for this study. Meniscal size also increased in the control group, and the difference of meniscal size between the two groups disappeared at 12 weeks; however, the synovium-MSC injected groups showed better results from the standpoint of type II collagen expression and electron microscopic features.

For clinical application, interspecies differences have to be considered. The inherent healing capacity of the meniscus has been shown to be lacking in the inner third and is very limited in the middle third of this poorly vascularized tissue in humans [29] and dogs [30]. We used a rat model, and rat meniscus had a greater spontaneous healing potential. To demonstrate the effectiveness of intra-articular injection of synovium-MSCs for meniscus regeneration, further experimental studies in larger animals are needed.

Native meniscus play an important role in knee stability and shock absorption [31], and this property is linked to the biphasic microstructure of the meniscus [32]. The extracellular matrix of the meniscus is composed mainly of collagen, with smaller quantities of proteoglycans, matrix glycoproteins, and elastin [33]. In this study, we showed that in the synovium-MSC injection group, the menisci regenerated much better than it did in the control group morphologically, and synovium-MSC injection prevented cartilage degeneration at 12 weeks after the meniscectomy as shown in Figure 3F. However, our data lack the details about biomechanical and biochemical properties of regenerated tissues, and it is still uncertain whether the regenerated menisci function in a normal manner and prevent secondary osteoarthritic change in the long term. Therefore, future studies should include biomechanical and biochemical analysis of the regenerated menisci.

Recently, we reported that human synovium-MSCs increased in synovial fluid after intra-articular ligament injury and that exogenous synovium-MSCs adhered to the injured ligament in a rabbit model [6, 34]. We also demonstrated that autologous synovial fluid enhanced migration of MSCs from synovium of osteoarthritis patients in a tissue culture system seemingly to delay the progression of the cartilage degeneration [7]. We speculate that synovial tissue may serve as a reservoir of stem cells that mobilize following intra-articular tissue injury and migrate to the site to participate in the repair response.

According to our speculation, in the case of meniscus injury, MSCs are mobilized from synovium into synovial fluid, and these cells adhere to the injured meniscus. However, the number of MSCs suspended in the synovial fluid and attached to the site is too low to repair or regenerate the injured meniscus, explaining poor spontaneous healing potential of meniscus. Intra-articular injection of synovium-MSCs can boost natural healing ability for meniscal regeneration.

Intravenous infusion of synovium-MSCs may be another route for administration. Although promising results were reported with i.v. infusion of bone marrow-MSCs in animal disease models [35], contrary views are also reported showing that a large fraction of intravenously infused bone marrow-MSCs are trapped in the lung [36]. Cell therapy for meniscal injury has an advantage in that intra-articular injection is possible instead of systemic injection.

The meniscal-deficient knee is a common problem faced by orthopedic surgeons. Although repair of meniscal lesions is possible in selected cases, the poor healing capacity of the tissue often dictates meniscectomy, the most common treatment for meniscal injury. Although meniscectomy provides pain relief and return to function, the loss of meniscal tissue results in long-term dysfunction and secondary osteoarthritis. Currently, there are multiple strategies for addressing this objective, including meniscal allografts, biologic scaffolds for tissue-engineered replacement tissue, and biologic stimuli for meniscal tissue regeneration. In this study, we focused on meniscal regeneration by using synovium-MSCs. Our method has a possibility of regenerating meniscus with less invasion in comparison with meniscal transplantation.

Conclusion

Synovium-MSCs injected into the massive meniscectomized knee adhered to the lesion, differentiated into meniscal cells

directly, and promoted meniscal regeneration without mobilization to distant organs.

ACKNOWLEDGMENTS

We thank Miyoko Ojima for expert help with histology, Yasuko Sakuma for help with animal experiments, and Noriko Hashimoto for skillful technical assistance with microarray and real-time PCR analyses. This study was supported by grants from "the Japan Society for the Promotion of Science (16591478)" to I.S. and "the Japanese Ministry of Education Global Center of Excellence (GCOE) Program, International Research Center for Molecular Science in Tooth and Bone Diseases" to T.M.

DISCLOSURE OF POTENTIAL CONFLICTS OF INTEREST

The authors indicate no potential conflicts of interest.

REFERENCES

1 Wieland HA, Michaelis M, Kirschbaum BJ et al. Osteoarthritis—An untreatable disease? Nat Rev Drug Discov 2005;4:331–344.
2 Chen FH, Rousche KT, Tuan RS. Technology insight: Adult stem cells in cartilage regeneration and tissue engineering. Nat Clin Pract Rheumatol 2006;2:373–382.
3 Ratajczak W. Early development of the cruciate ligaments in staged human embryos. Folia Morphol (Warsz) 2000;59:285–290.
4 Sakaguchi Y, Sekiya I, Yagishita K et al. Comparison of human stem cells derived from various mesenchymal tissues: Superiority of synovium as a cell source. Arthritis Rheum 2005;52:2521–2529.
5 Yoshimura H, Muneta T, Nimura A et al. Comparison of rat mesenchymal stem cells derived from bone marrow, synovium, periosteum, adipose tissue, and muscle. Cell Tissue Res 2007;327:449–462.
6 Morito T, Muneta T, Hara K et al. Synovial fluid-derived mesenchymal stem cells increase after intra-articular ligament injury in humans. Rheumatology (Oxford) 2008;47:1137–1143.
7 Zhang S, Muneta T, Morito T et al. Autologous synovial fluid enhances migration of mesenchymal stem cells from synovium of osteoarthritis patients in tissue culture system. J Orthop Res 2008;26: 1413–1418.
8 Hakamata Y, Murakami T, Kobayashi E. "Firefly rats" as an organ/cellular source for long-term in vivo bioluminescent imaging. Transplantation 2006;81:1179–1184.
9 Inoue H, Ohsawa I, Murakami T et al. Development of new inbred transgenic strains of rats with LacZ or GFP. Biochem Biophys Res Commun 2005;329:288–295.
10 Sekiya I, Larson BL, Vuoristo JT et al. Adipogenic differentiation of human adult stem cells from bone marrow stroma (MSCs). J Bone Miner Res 2004;19:256–264.
11 Sekiya I, Vuoristo JT, Larson BL et al. In vitro cartilage formation by human adult stem cells from bone marrow stroma defines the sequence of cellular and molecular events during chondrogenesis. Proc Natl Acad Sci USA 2002;99:4397–4402.
12 Kato A, Homma T, Batchelor J et al. Interferon-α/β receptor-mediated selective induction of a gene cluster by CpG oligodeoxynucleotide 2006. BMC Immunol 2003;4:8.
13 Quackenbush J. Computational analysis of microarray data. Nat Rev Genet 2001;2:418–427.
14 Contag PR, Olomu IN, Stevenson DK et al. Bioluminescent indicators in living mammals. Nat Med 1998;4:245–247.
15 Ichinose S, Tagami M, Muneta T et al. Morphological examination during in vitro cartilage formation by human mesenchymal stem cells. Cell Tissue Res 2005;322:217–226.
16 Murphy JM, Fink DJ, Hunziker EB et al. Stem cell therapy in a caprine model of osteoarthritis. Arthritis Rheum 2003;48:3464–3474.
17 Caplan AI, Dennis JE. Mesenchymal stem cells as trophic mediators. J Cell Biochem 2006;98:1076–1084.
18 Abdel-Hamid M, Hussein MR, Ahmad AF et al. Enhancement of the repair of meniscal wounds in the red-white zone (middle third) by the injection of bone marrow cells in canine animal model. Int J Exp Pathol 2005;86:117–123.
19 Agung M, Ochi M, Yanada S et al. Mobilization of bone marrow-derived mesenchymal stem cells into the injured tissues after intra-articular injection and their contribution to tissue regeneration. Knee Surg Sports Traumatol Arthrosc 2006;14:1307–1314.
20 Ochi M, Uchio Y, Okuda K et al. Expression of cytokines after meniscal rasping to promote meniscal healing. Arthroscopy 2001;17: 724–731.
21 Nimura A, Muneta T, Koga H et al. Increased proliferation of human synovial mesenchymal stem cells with autologous human serum: comparisons with bone marrow mesenchymal stem cells and with fetal bovine serum. Arthritis Rheum 2008;58:501–510.
22 Wakitani S, Takaoka K, Hattori T et al. Embryonic stem cells injected into the mouse knee joint form teratomas and subsequently destroy the joint. Rheumatology (Oxford) 2003;42:162–165.
23 Takahashi K, Yamanaka S. Induction of pluripotent stem cells from mouse embryonic and adult fibroblast cultures by defined factors. Cell 2006;126:663–676.
24 Koga H, Shimaya M, Muneta T et al. Local adherent technique for transplanting mesenchymal stem cells as a potential treatment of cartilage defect. Arthritis Res Ther 2008;10:R84.
25 Koga H, Muneta T, Ju YJ et al. Synovial stem cells are regionally specified according to local microenvironments after implantation for cartilage regeneration. Stem Cells 2007;25:689–696.
26 Segawa Y, Muneta T, Makino H et al. Mesenchymal stem cells derived from synovium, meniscus, anterior cruciate ligament, and articular chondrocytes share similar gene expression profiles. J Orthop Res 2008 [Epub ahead of print].
27 Koga H, Muneta T, Nagase T et al. Comparison of mesenchymal tissues-derived stem cells for in vivo chondrogenesis: Suitable conditions for cell therapy of cartilage defects in rabbit. Cell Tissue Res 2008; 333:207–215.
28 Mizuno K, Muneta T, Morito T et al. Exogenous synovial stem cells adhere to defect of meniscus and differentiate into cartilage cells. J Med Dent Sci 2008;55:101–111.
29 Cannon WD Jr., Vittori JM. The incidence of healing in arthroscopic meniscal repairs in anterior cruciate ligament-reconstructed knees versus stable knees. Am J Sports Med 1992;20:176–181.
30 Arnoczky SP, Warren RF. The microvasculature of the meniscus and its response to injury. An experimental study in the dog. Am J Sports Med 1983;11:131–141.
31 Bendjaballah MZ, Shirazi-Adl A, Zukor DJ. Biomechanics of the human knee joint in compression: Reconstruction, mesh generation and finite element analysis. Knee 1995;2:69–79.
32 Gabrion A, Aimedieu P, Laya Z et al. Relationship between ultrastructure and biomechanical properties of the knee meniscus. Surg Radiol Anat 2005;27:507–510.
33 McDevitt CA, Webber RJ. The ultrastructure and biochemistry of meniscal cartilage. Clin Orthop Relat Res 1990;8–18.
34 McGonagle D, Jones E. A potential role for synovial fluid mesenchymal stem cells in ligament regeneration. Rheumatology (Oxford) 2008;47:1114–1116.
35 Iso Y, Spees JL, Serrano C et al. Multipotent human stromal cells improve cardiac function after myocardial infarction in mice without long-term engraftment. Biochem Biophys Res Commun 2007;354: 700–706.
36 Lee RH, Seo MJ, Pulin AA et al. The CD34-like protein PODXL and {alpha}6-integrin (CD49f) identify early progenitor MSCs with increased clonogenicity and migration to infarcted heart in mice. Blood 2009;113:816–826.

Biochemical and Biophysical Research Communications 378 (2009) 600–604

Contents lists available at ScienceDirect

Biochemical and Biophysical Research Communications

journal homepage: www.elsevier.com/locate/ybbrc

Latexin is involved in bone morphogenetic protein-2-induced chondrocyte differentiation

Ichiro Kadouchi [a,b], Kei Sakamoto [b], Liu Tangjiao [b,c], Takashi Murakami [d], Eiji Kobayashi [d], Yuichi Hoshino [a], Akira Yamaguchi [b,e,*]

[a] Department of Orthopedic Surgery, Jichi Medical University, Shimotsuke, Tochigi, Japan
[b] Section of Oral Pathology, Department of Oral Restitution, Graduate School of Tokyo Medical and Dental University, Bunkyo-ku, Tokyo 113-8549, Japan
[c] Section of Oral Pathology, College of Stomatology, Dalian Medical University, Dalian, China
[d] Division of Organ Replacement Research, Center for Molecular Medicine, Jichi Medical University, Shimotsuke, Tochigi, Japan
[e] Global Center of Excellence Program, International Research Center for Molecular Science in Tooth and Bone Diseases, Graduate School of Tokyo Medical and Dental University, Bunkyo-ku, Tokyo 113-8549, Japan

ARTICLE INFO

Article history:
Received 17 November 2008
Available online 4 December 2008

Keywords:
Latexin
BMP-2
Chondrocyte
Bone regeneration
Cartilage
Bone fracture

ABSTRACT

Latexin is the only known carboxypeptidase A inhibitor in mammals. We previously demonstrated that BMP-2 significantly induced *latexin* expression in Runx2-deficient mesenchymal cells (RD-C6 cells), during chondrocyte and osteoblast differentiation. In this study, we investigated latexin expression in the skeleton and its role in chondrocyte differentiation. Immunohistochemical studies revealed that proliferating and prehypertrophic chondrocytes expressed latexin during skeletogenesis and bone fracture repair. In the early phase of bone fracture, *latexin* mRNA expression was dramatically upregulated. BMP-2 upregulated the expression of the mRNAs of *latexin*, *Col2a1*, and the gene encoding aggrecan (*Agc1*) in a micromass culture of C3H10T1/2 cells. Overexpression of *latexin* additively stimulated the BMP-2-induced expression of the mRNAs of *Col2a*, *Agc1*, and *Col10a1*. BMP-2 treatment upregulated *Sox9* expression, and *Sox9* stimulated the promoter activity of *latexin*. These results indicate that latexin is involved in BMP-2-induced chondrocyte differentiation and plays an important role in skeletogenesis and skeletal regeneration.

Chondrocytes and osteoblasts originate from common progenitors called mesenchymal stem cells [1]. During the differentiation of these cells, bone morphogenetic proteins (BMPs) play a crucial role in inducing the expression of lineage-specific transcription factors such as Runx2 [1–3] and Sox9 [4,5]; Runx2 is an essential transcription factor that regulates osteoblast differentiation [1,6,7] and chondrocyte maturation [8], and Sox9 is an important transcription factor that regulates chondrocyte differentiation from mesenchymal stem cells [5,9].

We established a clonal cell line, RD-C6, from *Runx2*-deficient mouse embryos and demonstrated that this cell line could differentiate into both osteoblasts and chondrocytes in response to BMP-2 treatment via a Runx2-independent pathway [10]. By microarray analysis of this cell line with and without BMP-2 treatment, we identified latexin as a downstream factor of BMP-2 signaling [10]. This implied that latexin expression was regulated by BMP-2 signaling via a Runx2-independent pathway.

Latexin is composed of 222 amino acids and has a molecular weight of 29 kDa; further, it is the only known carboxypeptidase A inhibitor in mammals [11,12]. The latexin was discovered in the lateral neocortex of rats, and it acts as a marker of regionality and development of both the central and the peripheral nervous systems [11]. Further, *latexin* is expressed in several other tissues, including hematopoietic and lymphoid organs, and plays an important role in regulating the activity of hematopoietic stem cells [12,13]. By microarray analysis, Balint et al. [14] briefly mentioned that *latexin* was one of the upregulated genes in BMP-2-treated C2C12 cells. This suggests a possible role of latexin in osteoblast differentiation, because C2C12 cells exclusively differentiated into osteoblasts and not into chondrocytes by BMP-2 treatment [15]. In addition, we demonstrated that BMP-2 induced RD-C6 cells to differentiate into both osteoblast and chondrocyte lineage cells [10]. However, it remained unclear whether latexin is involved in osteogenic differentiation, chondrogenic differentiation, or both.

To investigate the role of latexin in skeletal cell differentiation, we first investigated latexin expression during skeletogenesis and skeletal regeneration and examined its role in chondrocyte differentiation by using a multipotent mesenchymal cell line, C3H10T1/2. Here, we describe that latexin is expressed in chondrocytes and involved in BMP-2-induced chondrocyte differentiation.

* Corresponding author. Address: Section of Oral Pathology, Department of Oral Restitution, Graduate School of Tokyo Medical and Dental University, Bunkyo-ku, Tokyo 113-8549, Japan. Fax: +81 3 5803 0188.
E-mail address: akira.mpa@tmd.ac.jp (A. Yamaguchi).

0006-291X/$ - see front matter © 2008 Elsevier Inc. All rights reserved.
doi:10.1016/j.bbrc.2008.11.111

Materials and methods

Immunohistochemistry. Immunohistochemical staining was performed on 4% paraformaldehyde-fixed, ethylenediaminetetraacetic acid (EDTA)-decalcified, and paraffin-embedded sections. Endogenous peroxidase activity was blocked with 10% hydrogen peroxidase/methanol, and nonspecific binding was blocked with 10% horse serum. The sections were incubated with goat anti-latexin (Everest Biotech, Oxfordshire, UK) or rabbit anti-Sox9 (Santa Cruz Biotechnology Inc., Santa Cruz, CA) overnight at 4 °C. After washing, they were incubated with horseradish peroxidase-conjugated secondary antibodies (Dako, Glostrup, Denmark). The antigen-bound peroxidase activity was visualized by staining the sections with 3-amino-9-ethyl-carbazole (AEC) chromogen.

Fracture model. The midshafts of the tibiae of 8-week-old mice were fractured using a bone saw and internally stabilized with an intramedullary nail by using the inner pin of a spinal needle with 22-G diameter. The mice were sacrificed and submitted for histological and real-time reverse-transcriptase polymerase chain reaction (RT-PCR) analyses on 5, 10, and 15 days after the operation. All animal studies were approved by the Animal Ethics Committee of Jichi Medical University and performed in accordance with the Jichi Medical University Guide for the Care and Use of Laboratory Animals, following the principles of laboratory animal care formulated by the National Society for Medical Research.

Cell culture. C3H10T1/2 (clone 8) cells were purchased from Cell Bank, RIKEN BioResource Center (Tsukuba, Japan). The cells were maintained in Eagle's basal medium containing 10% fetal bovine serum (FBS; Sigma, St. Louis, MO), 1-glutamine, 50 U/ml penicillin G, and 50 mg/ml streptomycin. For a micromass culture, the C3H10T1/2 cells were suspended in the medium at a concentration of 1×10^7 cells/ml, and a 10-μl drop of this cell suspension was placed in the center of a culture dish. The cells were allowed to adhere for 3 h, and a medium with or without recombinant human BMP-2 (rhBMP-2; 100 ng/ml; Astellas Pharma Inc., Tokyo, Japan) was added to the culture. The cells were stained with Alcian blue solution (pH 2.5) on days 2 and 4 *in vitro*.

Mouse cDNA containing *latexin* open reading frame was obtained by PCR and subcloned into pMSCV (Clontech, CA). Retrovirus was produced and cells were infected with the retrovirus according to the manufacturer's instructions. After infection, the cells were selected in a puromycin-containing medium for 2 weeks.

Western blot analysis. The cells were lysed with radioimmunoprecipitation assay (RIPA) buffer containing protease inhibitor cocktail (Roche Diagnostics, Basel, Switzerland). Western blot analysis was performed according to the standard procedure. SDS–polyacrylamide gel electrophoresis (PAGE) was performed using 1× sample buffer containing 5% β-mercaptoethanol. The proteins were transferred to nitrocellulose membranes, which were then incubated with the following primary antibodies for 1 h: goat anti-latexin, rabbit anti-Sox9, and anti-actin (SC-1616; Santa Cruz Biotechnology Inc.). Next, the membranes were incubated with the respective secondary antibodies for 1 h. Chemiluminescence was detected with an enhanced chemiluminescence (ECL) Plus chemiluminescence detection kit (GE Healthcare, UK).

Real-time RT-PCR. Total RNA was extracted from the cultured cells using RNA Smart Total RNA Isolation Kit (Macherey-Nagel GmbH & Co. KG, Düren, Germany). RNA aliquots of 500 ng were reverse transcribed to cDNA by using a First-Strand cDNA synthesis kit for RT-PCR (Invitrogen Corp., Carlsbad, CA) and an oligo-dT primer. mRNA expression was quantified by real-time RT-PCR, using a MiniOpticon system (Bio-Rad Laboratories, Hercules, CA) with the iQ SYBR Green supermix (Bio-Rad Laboratories). Relative amount of each mRNA was normalized to 18 S rRNA expression. The primer sequences are listed in Table 1.

Table 1
Primers used for real-time-based RT-PCR.

	Forward primer	Reverse primer
Lxn	5′- GTCGCCTGCGGTTATGTAAT	5′- GGCGGCTGTTGTGTTTTACT
Col2a1	5′-TGCACGAAACACACTGGTAAG	5′- CACCAAATTCCTGTTCAGCC
Agc1	5′- AGGAGACCCAGACAGCAGAA	5′-ACAGTGACCCTGGAACTTGG
Col10a1	5′-TGGGTAGGCCTGTATAAAGAACGG	5′-CATGGGAGCCACTAGGAATCC TGAGA
Sox9	5′- CTCGCAATACGACTACGCT	5′-CTGGTTGTTCCCAGTGCT
18S rRNA	5′-GTAACCCGTTGAACCCCATT	5′-CCATCCAATCGGTAGTAGCG

Luciferase activity assay. The proximal promoter region of human *latexin* was obtained from a bacterial artificial chromosome (BAC) clone, RP11-bA39F4, by PCR, and the product was cloned into pGL3-basic (latexin-luc; Promega, Madison, WI). The latexin-luc plasmid was transfected into C3H10T1/2 cells, using Lipofectamine 2000 (Invitrogen) according to the manufacturer's instructions. The amount of latexin-luc plasmid was 0.5 μg in every experiment. Luciferase activity was measured 48 hours after the transfection by using a luciferase assay kit (Promega) according to the manufacturer's instructions.

Statistics. Statistical analyses were performed using Student's unpaired *t*-test. Each experiment was conducted at least twice. The data presented represent means ± standard deviation (SD) of independent replicates ($n > 3$).

Results

Some chondrocytes express latexin in embryonic skeleton and regenerative bone

We first investigated latexin expression during skeletogenesis in embryonic mice and skeletal regeneration in adult mice by immunohistochemistry. Latexin expression was observed in resting to prehypertrophic chondrocytes but not in hypertrophic chondrocytes in E15.5 embryos (Fig. 1A and B). The distribution of latexin-positive cells was similar to that of Sox9-positive cells (Fig. 1C and D). Some osteoblastic cells at periosteoal region in bone collar showed weak signals for latexin expression (Fig. 1A). The peripheral nerves at perichondral membrane exhibited strong signals of latexin (Fig. 1A).

We next examined latexin expression during bone fracture healing at the tibial diaphyses by immunohistochemistry (Fig. 1E–J). In our experimental model, chondrocytes appeared at the periosteal region around the bone fracture site on day 5 after the injury (Fig. 1E). Immunohistochemical studies revealed that many of these chondrocytes were positive for latexin (Fig. 1F). Interestingly, immunoreactivity was detected in the nuclei as well as the cytoplasm of numerous chondrocytes. Numerous hypertrophic chondrocytes and newly formed trabecular bones were observed on day 10, but only proliferating or prehypertrophic chondrocytes were positive for latexin (Fig. 1G and H). Hypertrophic chondrocytes showed no apparent signals for latexin expression (Fig. 1H). On day 15, the process of new bone formation progressed by replacing the preexisting cartilage (Fig. 1I), and osteoblasts covering newly formed bone trabeculae showed no apparent signals of latexin (Fig. 1J). The number of latexin-positive cells dramatically decreased on day 15 as compared with those on days 5 and 10. No apparent signals were found in the osteoblastic cells covering the trabecular and cortical bones away from fracture sites.

Real-time RT-PCR analysis confirmed that *latexin* expression was undetectable before the injury; however, its expression dramatically increased on day 5 after the injury and then gradually declined on days 10 and 15 (Fig. 1K).

These results indicate that latexin is expressed in chondrogenic cells during skeletogenesis in mouse embryos, and its expression is

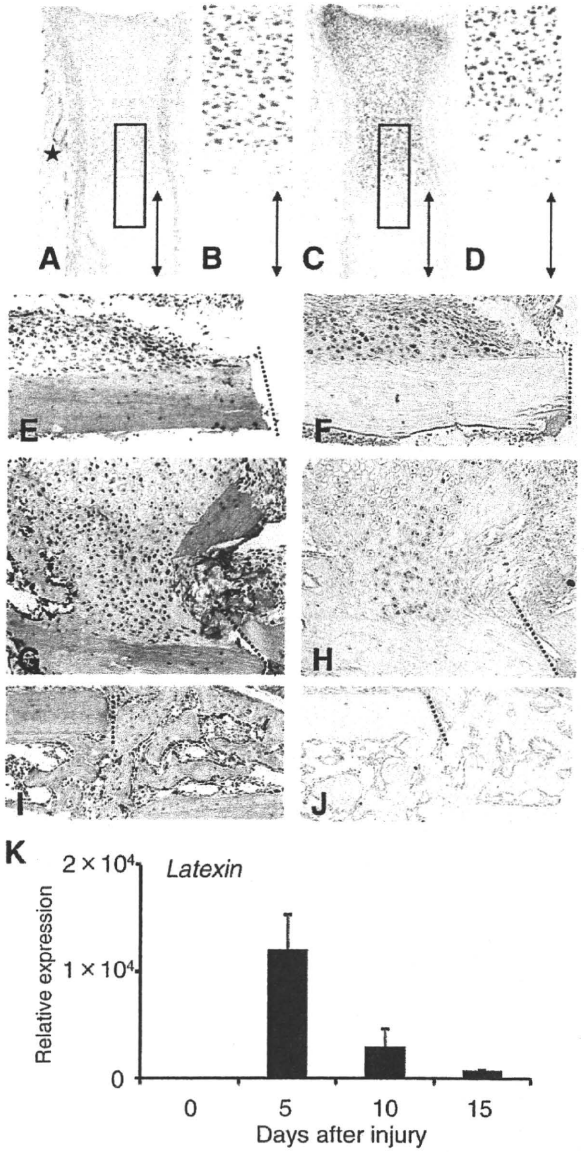

Fig. 1. Chondrocytes express latexin expression in the embryonic tibiae (A,B) and during skeletal regeneration in adult mice (F, H, and J). (A,B) Immunohistochemical staining of latexin in the tibia of an E15.5 mouse embryo. A higher magnification image of the square in A is shown in B. (C,D) Immunohistochemical staining of Sox9 in the tibia of an E15.5 mouse embryo. A higher magnification image of the square in C is shown in D. Arrows in A, B, C, and D indicate hypertrophic chondrocytes zones. An asterisk in A shows latexin-positive peripheral nerves. (E, G, and I) Hematoxylin–eosin staining images of fracture repair on days 5 (E), 10 (G) and 15 (I) after injury in tibiae of adult mice. (F, H, and J) Immunohistochemical staining of latexin during fracture repair. Note that latexin-positive chondrocytes in F and H. Hypertrophic chondrocytes in H and osteoblasts covering newly formed bone trabeculae exhibit few signals for latexin. Dotted lines in E–J indicate fracture end of cortical bones. (K) *Latexin* mRNA expression during fracture repair assessed by real-time RT-PCR as described in Materials and methods.

limited to the chondrocytes appearing during fracture repair in adult mice.

BMP-2 induces latexin expression in C3H10T1/2 cells along with chondrocyte differentiation

To investigate the role of latexin in chondrocyte differentiation, we used a micromass culture of C3H10T1/2 cells. The cultured cells produced Alcian blue-positive extracellular matrix on day 2, the amount of which increased on day 4 in the culture (Fig. 2A). BMP-2 treatment increased the production of Alcian blue-positive extracellular matrix on days 2 and 4 as compared with the respective control cultures (Fig. 2A). The treatment significantly increased the *in vitro* expression of the mRNA for *Col2a1* and *aggrecan* (*Agc1*), which encode the major components of extracellular matrices synthesized by chondrocytes, on days 2 and 4 (Fig. 2B). These results indicate that C3H10T1/2 cells maintained in a micromass culture differentiate into chondrogenic cells in response to BMP-2. We next investigated *latexin* expression in C3H10T1/2 cells cultured in this system by real-time RT-PCR and Western blot analysis. BMP-2 upregulated the latexin expression on days 2 and 4 at the mRNA and protein levels (Fig. 2C and D). These results suggest that BMP-2 induces latexin expression along with chondrocyte differentiation.

Overexpression of latexin stimulates BMP-2-induced chondrocyte differentiation

We overexpressed mouse *latexin* gene in C3H10T1/2 cells by infecting the cells with a retrovirus. The infected cells were cultured with and without rhBMP-2 for 2 days. The cells overexpressing *latexin* induced no changes in the expression of the mRNAs of *Col2a1*, *Agc1*, and *Col10a1* in the absence of BMP-2, compared with the control culture (Fig. 3). In contrast, the cells overexpressing *latexin* significantly increased the expression of the abovementioned mRNAs in the presence of BMP-2, as compared with the BMP-2-treated cells transduced with green fluorescent protein (GFP) (Fig. 3). These results suggest that latexin additively stimulates BMP-2-induced chondrocyte differentiation.

Sox9 stimulates the promoter activity of latexin

BMP-2 induced *latexin* expression in RD-C6 cells, Runx2-deficient cell line, as well as in C3H10T1/2 cells. These results prompted us to investigate whether BMP-2 directly stimulated the promoter activity of *latexin*, and we found that BMP-2 treatment induced no apparent stimulation of the promoter activity of *latexin* at concentrations of 100 and 500 ng/ml (data not shown). It has been reported that BMP-2 efficiently induces *Sox9* expression along with chondrogenic differentiation [4,5], and we also confirmed BMP-2-induced upregulation of *Sox9* mRNA expression in C3H10T1/2 cells on day 2 (Fig. 4A). Therefore, we investigated whether *Sox9* regulates the promoter activity of *latexin*. As shown in Fig. 4B, Sox9 stimulated the promoter activity of *latexin*. These findings suggest that BMP-2-induced Sox9 regulates *latexin* expression in chondrogenic differentiation.

Discussion

Latexin is expressed in various tissues, including brain tissues and hematopoietic and lymphoid organs [11–13,16,17], but its expression and function in skeletal tissues have not been reported in detail. We previously identified *latexin* as a downstream factor of BMP signaling by a microarray analysis of RD-C6 cells, a Runx2-deficient cell line, with and without BMP-2 treatment [10]. Since BMP-2 treatment induced RD-C6 cells to differentiate into both osteoblasts and chondrocytes [10], we first investigated latexin expression during skeletogenesis and skeletal regeneration to identify the skeletal cells that express latexin *in vivo* by immunohistochemistry. This study revealed that the proliferating and pre-hypertrophic chondrocytes in the embryonic tibiae and callus appearing during skeletal regeneration in adult mice expressed latexin. Real-time RT-PCR analysis also indicated the great induction

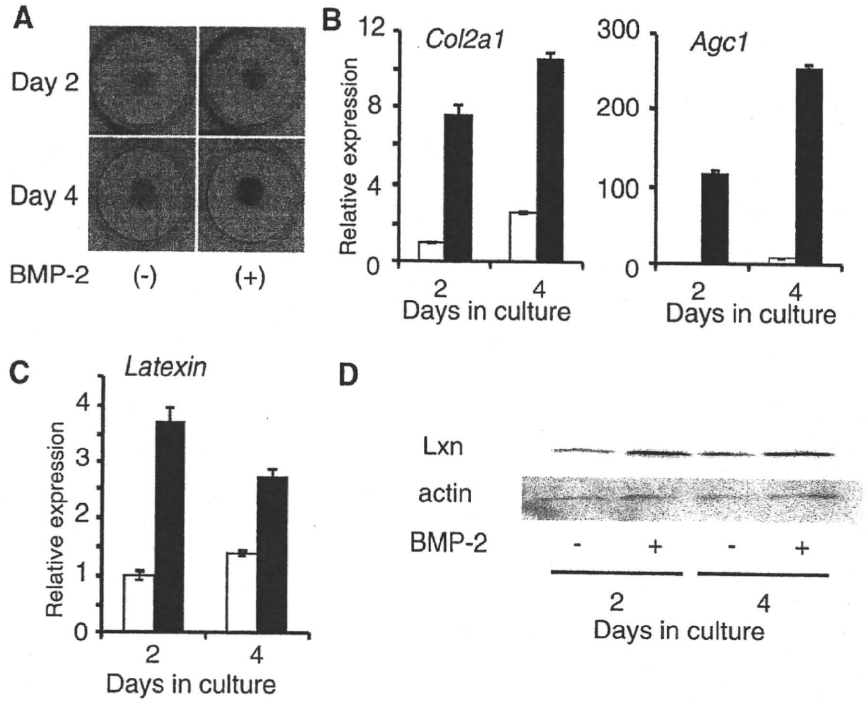

Fig. 2. BMP-2 stimulated the expression of *latexin* mRNA in a micromass culture of C3H10T1/2 cells along with chondrocyte differentiation. (A) Alcian blue staining of C3H10T1/2 cells cultured with and without BMP-2 (100 ng/ml) for 2 and 4 days. (B) Effects of BMP-2 on mRNA expression for *Col2a1* and *Agc1*. C3H10T1/2 cells were cultured for 2 and 4 days in the absence (open bars) and presence (closed bars) of BMP-2, and the expression of the abovementioned mRNAs was determined by real-time RT-PCR. (C) Effects of BMP-2 on the expression of *latexin* mRNA. C3H10T1/2 cells were cultured for 2 and 4 days in the absence (open bars) and presence (closed bars) of BMP-2. (D) Effects of BMP-2 on latexin expression. C3H10T1/2 cells were cultured for 2 and 4 days in the absence and presence of BMP-2, and latexin expression was examined by Western blot analysis as described in Materials and methods.

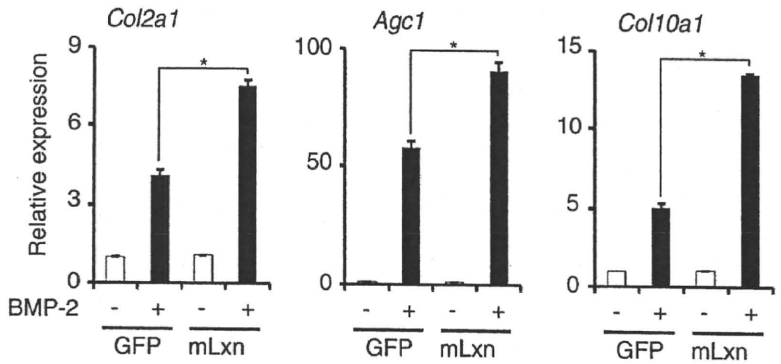

Fig. 3. Overexpression of latexin stimulated BMP-2-induced chondrocyte differentiation in a micromass culture of C3H10T1/2 cells. The cells were cultured for 2 days with and without BMP-2 (100 ng/ml). The expression of the mRNAs of *Col2a*, *Agc1*, and *Col10a1* were determined by real-time RT-PCR as described in Materials and methods). Relative amount of each mRNA was normalized to 18S rRNA expression. $^{*}P < 0.05$ versus control cells.

of *latexin* mRNA expression in the early phase of skeletal regeneration. Taken together, these results suggest that latexin plays an important role in skeletogenesis and skeletal regeneration.

These immunohistochemical findings prompted us to investigate the role of latexin in chondrocyte differentiation, for which we used a micromass culture of C3H10T1/2 cells. The culture experiments revealed that the expression of *latexin* mRNA correlated with that of other chondrocyte differentiation-related mRNAs such as those of *Col2a1* and *Agc1*. In addition, overexpression of *latexin* additively stimulated BMP-2-induced chondrocyte differentiation. Interestingly, overexpression of latexin induced no significant changes in the expression of the abovementioned mRNAs in the absence of BMP-2, suggesting a close interaction between the regulation of *latexin* expression and BMP signaling. To further investigate the underlying mechanism, we examined the effects of BMP-2 on the activation of *latexin* promoter and found that BMP-2 did not stimulate the promoter. Since it has been reported that BMP-2 induces Sox9 expression [4,5], we examined the effects of *Sox9* on the transactivation of *latexin* promoter and demonstrated that *Sox9* stimulated the promoter activity of *latexin*. These results suggest that latexin is involved in chondrocyte differentiation via Sox9, the expression of which is upregulated by BMP-2. There have been no reports about the regulatory mechanism of *latexin* expression even in neural tissues, and *Sox9* is the first candidate transcription factor that regulates *latexin* expression. However, its *latexin*-transducing activity was not observed to be

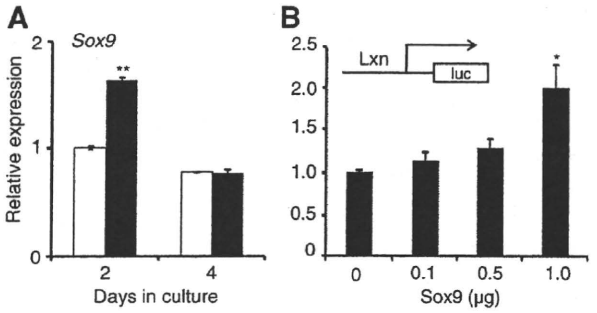

Fig. 4. BMP-2 induced the expression of *Sox9* mRNA in C3H10T1/2 cells, and Sox9 activated the promoter activity of *latexin*. (A) Effects of BMP-2 on the expression of *Sox9* mRNA in C3H10T1/2 cells on day 2, determined by real-time RT-PCR analysis. $^{**}P < 0.0001$ versus control cells. (B) Effect of Sox9 on the promoter activity of *latexin*. Data represent the fold inductions relative to the induction by mock vector transfection. $^{*}P < 0.05$ versus control cells.

strong. These findings suggest that activation of *latexin* transcription requires other transcription factors or coactivators of Sox9 such as Sox5, Sox6, and cAMP response element binding (CREB)-binding protein (CBP)/p300 [18–21].

Latexin is the only known endogenous carboxypeptidase A inhibitor in mammals [12]. It is structurally composed of two nearly identical domains that have a high conformational homology with the cystatins [22]. *Latexin* has the potential heparin/heparan sulfate-binding sites and directly interacts with a heparin component in a mast cell culture [22,16]. Heparan sulfate is an important component of the extracellular matrix of cartilage and essential for chondrocyte differentiation [23,24]. This suggests an interaction between latexin and heparan sulfate during extracellular matrix synthesis in cartilage. Our immunohistochemical study revealed the nuclear localization of latexin in chondrocytes appearing during fracture repair. It will be interesting to investigate the interaction between latexin and heparan sulfate in the nuclei, because some reports have indicated the nuclear localization of heparin sulfate [25].

In the present study, we demonstrated that latexin is expressed in chondrocytes during skeletogenesis and skeletal regeneration. *Latexin*-deficient mice, which were provided by Dr. Arimitsu [26], exhibited no growth retardation or apparent radiographic changes in the skeleton (unpublished results), suggesting the limited changes in the skeletal tissues of the mice. Since the present study revealed the dramatic upregulation of *latexin* mRNA expression in the early phase of fracture repair, it will be interesting to investigate the process of fracture repair in *latexin*-deficient mice. Such studies are currently being conducted by our group. The findings of these studies will provide important information regarding the role of latexin in skeletal growth and regeneration.

Acknowledgments

This work was supported by the Research Award to Jichii Medical University Graduate Student (I.K.) and a Grant-in-Aid for Scientific Research from the Japan Society for the Promotion of Science (A.Y.).

References

[1] A. Yamaguchi, T. Komori, T. Suda, Regulation of osteoblast differentiation mediated by bone morphogenetic proteins, hedgehogs, and Cbfa1, Endocr. Rev. 21 (2000) 393–411.
[2] K.S. Lee, H.J. Kim, Q.L. Li, X.Z. Chi, C. Ueta, T. Komori, J.M. Wozney, E.G. Kim, J.Y. Choi, H.M. Ryoo, S.C. Bae, Runx2 is a common target of transforming growth factor beta1 and bone morphogenetic protein 2, and cooperation between Runx2 and Smad5 induces osteoblast-specific gene expression in the pluripotent mesenchymal precursor cell line C2C12, Mol. Cell. Biol. 20 (2000) 8783–8792.
[3] M.H. Lee, Y.J. Kim, H.J. Kim, H.D. Park, A.R. Kang, H.M. Kyung, J.H. Sung, J.M. Wozney, H.M. Ryoo, BMP-2-induced Runx2 expression is mediated by Dlx5, and TGF-beta 1 opposes the BMP-2-induced osteoblast differentiation by suppression of Dlx5 expression, J. Biol. Chem. 278 (2003) 34387–34394.
[4] B.K. Zehentner, C. Dony, H. Burtscher, The transcription factor Sox9 is involved in BMP-2 signaling, J. Bone Miner. Res. 14 (1999) 1734–1741.
[5] M.B. Goldring, K. Tsuchimochi, K. Ijiri, The control of chondrogenesis, J. Cell Biochem. 97 (2006) 33–44.
[6] T. Komori, H. Yagi, S. Nomura, A. Yamaguchi, K. Sasaki, K. Deguchi, Y. Shimizu, R.T. Bronson, Y.H. Gao, M. Inada, M. Sato, R. Okamoto, Y. Kitamura, S. Yoshiki, T. Kishimoto, Targeted disruption of Cbfa1 results in a complete lack of bone formation owing to maturational arrest of osteoblasts, Cell 89 (1997) 755–764.
[7] P. Ducy, R. Zhang, V. Geoffroy, A.L. Ridall, G. Karsenty, Osf2/Cbfa1: a transcriptional activator of osteoblast differentiation, Cell 89 (1997) 747–754.
[8] C.A. Yoshida, T. Furuichi, T. Fujita, R. Fukuyama, N. Kanatani, S. Kobayashi, M. Satake, K. Takada, T. Komori, Core-binding factor beta interacts with Runx2 and is required for skeletal development, Nat. Genet. 32 (2002) 633–638.
[9] H. Akiyama, Control of chondrogenesis by the transcription factor Sox9, Mod. Rheumatol. 18 (2008) 213–219.
[10] T. Liu, Y. Gao, K. Sakamoto, T. Minamizato, K. Furukawa, T. Tsukazaki, Y. Shibata, K. Bessho, T. Komori, A. Yamaguchi, BMP-2 promotes differentiation of osteoblasts and chondroblasts in Runx2-deficient cell lines, J. Cell Physiol. 211 (2007) 728–735.
[11] Y. Arimatsu, Latexin: a molecular marker for regional specification in the neocortex, Neurosci. Res. 20 (1994) 131–135.
[12] Y. Liang, G. Van Zant, Aging stem cells, latexin, and longevity, Exp. Cell. Res. 314 (2008) 1962–1972.
[13] Y. Liang, M. Jansen, B. Aronow, H. Geiger, G. Van Zant, The quantitative trait gene latexin influences the size of the hematopoietic stem cell population in mice, Nat. Genet. 39 (2007) 178–188.
[14] E. Balint, D. Lapointe, H. Drissi, C. van der Meijden, D.W. Young, A.J. van Wijnen, J.L. Stein, G.S. Stein, J.B. Lian, Phenotype discovery by gene expression profiling: mapping of biological processes linked to BMP-2-mediated osteoblast differentiation, J. Cell Biochem. 89 (2003) 401–426.
[15] T. Katagiri, A. Yamaguchi, M. Komaki, E. Abe, N. Takahashi, T. Ikeda, V. Rosen, J.M. Wozney, A. Fujisawa-Sehara, T. Suda, Bone morphogenetic protein-2 converts the differentiation pathway of C2C12 myoblasts into the osteoblast lineage, J. Cell Biol. 127 (1994) 1755–1766.
[16] Y. Uratani, K. Takiguchi-Hayashi, N. Miyasaka, M. Sato, M. Jin, Y. Arimatsu, Latexin, a carboxypeptidase A inhibitor, is expressed in rat peritoneal mast cells and is associated with granular structures distinct from secretory granules and lysosomes, Biochem. J. 346 (Pt 3) (2000) 817–826.
[17] Y. Hatanaka, Y. Uratani, K. Takiguchi-Hayashi, A. Omori, K. Sato, M. Miyamoto, Y. Arimatsu, Intracortical regionality represented by specific transcription for a novel protein, latexin, Eur. J. Neurosci. 6 (1994) 973–982.
[18] H. Akiyama, M.C. Chaboissier, J.F. Martin, A. Schedl, B. de Crombrugghe, The transcription factor Sox9 has essential roles in successive steps of the chondrocyte differentiation pathway and is required for expression of Sox5 and Sox6, Genes Dev. 16 (2002) 2813–2828.
[19] T. Furumatsu, M. Tsuda, K. Yoshida, N. Taniguchi, T. Ito, M. Hashimoto, H. Asahara, Sox9 and p300 cooperatively regulate chromatin-mediated transcription, J. Biol. Chem. 280 (2005) 35203–35208.
[20] T. Ikeda, S. Kamekura, A. Mabuchi, I. Kou, S. Seki, T. Takato, K. Nakamura, H. Kawaguchi, S. Ikegawa, U.I. Chung, The combination of SOX5, SOX6, and SOX9 (the SOX trio) provides signals sufficient for induction of permanent cartilage, Arthritis. Rheum. 50 (2004) 3561–3573.
[21] Y. Han, V. Lefebvre, L-Sox5 and Sox6 drive expression of the aggrecan gene in cartilage by securing binding of Sox9 to a far-upstream enhancer, Mol. Cell. Biol. 28 (2008) 4999–5013.
[22] A. Aagaard, P. Listwan, N. Cowieson, T. Huber, T. Ravasi, C.A. Wells, J.U. Flanagan, S. Kellie, D.A. Hume, B. Kobe, J.L. Martin, An inflammatory role for the mammalian carboxypeptidase inhibitor latexin: relationship to cystatins and the tumor suppressor TIG1, Structure 13 (2005) 309–317.
[23] E. Arikawa-Hirasawa, H. Watanabe, H. Takami, J.R. Hassell, Y. Yamada, Perlecan is essential for cartilage and cephalic development, Nat. Genet. 23 (1999) 354–358.
[24] H.P. Sørensen, R.R. Vivès, C. Manetopoulos, R. Albrechtsen, M.C. Lydolph, J. Jacobsen, J.R. Couchman, U.M. Wewer, Heparan Sulfate Regulates ADAM12 through a molecular switch mechanism, J. Biol. Chem. 283 (2008) 31920–31932.
[25] M. Kobayashi, Y. Naomoto, T. Nobuhisa, T. Okawa, M. Takaoka, Y. Shirakawa, T. Yamatsuji, J. Matsuoka, T. Mizushima, H. Matsuura, M. Nakajima, H. Nakagawa, A. Rustgi, N. Tanaka, Heparanase regulates esophageal keratinocyte differentiation through nuclear translocation and heparan sulfate cleavage, Differentiation 74 (2006) 235–243.
[26] M. Jin, M. Ishida, Y. Katoh-Fukui, R. Tsuchiya, T. Higashinakagawa, S. Ikegami, Y. Arimatsu, Reduced pain sensitivity in mice lacking latexin, An inhibitor of metallocarboxypeptidases, Brain Res. 1075 (2006) 117–121.

Biochemical and Biophysical Research Communications 381 (2009) 339–344

Contents lists available at ScienceDirect

Biochemical and Biophysical Research Communications

journal homepage: www.elsevier.com/locate/ybbrc

Early exercise in spinal cord injured rats induces allodynia through TrkB signaling

Teruaki Endo [a], Takashi Ajiki [a], Hirokazu Inoue [a], Motoshi Kikuchi [b], Takashi Yashiro [b], Sueo Nakama [a], Yuichi Hoshino [a], Takashi Murakami [c], Eiji Kobayashi [c,*]

[a] Department of Orthopedic Surgery, Jichi Medical University, Shimotsuke, Tochigi 329-0498, Japan
[b] Division of Histology, Department of Anatomy, Jichi Medical University, Shimotsuke, Tochigi 329-0498, Japan
[c] Division of Organ Replacement Research, Center for Molecular Medicine, Jichi Medical University, 3311-1 Yakushiji, Shimotsuke, Tochigi 329-0498, Japan

ARTICLE INFO

Article history:
Received 9 February 2009
Available online 15 February 2009

Keywords:
Spinal cord injury
Assisted stepping exercise
Neuronal regeneration
Neuropathic pain
Allodynia
Brain-derived neurotrophic factor
Tropomyosin-related kinase B

ABSTRACT

Rehabilitation is important for the functional recovery of patients with spinal cord injury. However, neurological events associated with rehabilitation remain unclear. Herein, we investigated neuronal regeneration and exercise following spinal cord injury, and found that assisted stepping exercise of spinal cord injured rats in the inflammatory phase causes allodynia. Sprague–Dawley rats with thoracic spinal cord contusion injury were subjected to assisted stepping exercise 7 days following injury. Exercise promoted microscopic recovery of corticospinal tract neurons, but the paw withdrawal threshold decreased and C-fibers had aberrantly sprouted, suggesting a potential cause of the allodynia. Tropomyosin-related kinase B (TrkB) receptor for brain-derived neurotrophic factor (BDNF) was expressed on aberrantly sprouted C-fibers. Blocking of BDNF–TrkB signaling markedly suppressed aberrant sprouting and decreased the paw withdrawal threshold. Thus, early rehabilitation for spinal cord injury may cause allodynia with aberrant sprouting of C-fibers through BDNF–TrkB signaling.

Introduction

Rehabilitation is commonly considered for spinal cord injured patients. In particular, rehabilitation plays a very important role in preventing muscle contraction and joint stiffness in patients with spinal cord injury [1], leading to an improvement in the quality of life of the patient. While it may be impossible for patients to perform voluntary exercise, assisted stepping exercise with partial weight bearing, referred to as "Body Weight Supported Treadmill Training (BWSTT)", has been investigated in the clinical setting [2]. Indeed, it has been demonstrated that BWSTT can improve the locomotor capacity of spinal transected rats [3]. Our previous studies also showed that assisted stepping exercise yielded beneficial effects in terms of functional recovery in hindlimb transplanted rats [4]. Nonetheless, the significance of such early rehabilitation in patients following spinal cord injury in the inflammatory phase remains unclear, and little is known about the efficiency of early rehabilitation in terms of neurological symptoms.

Herein, we focused on investigating the relationship between early exercise following spinal cord injury and neuronal regeneration, and found that early assisted stepping exercise for spinal cord injured rats promoted neuronal regeneration but caused allodynia with aberrant sprouting of C-fibers through BDNF–TrkB signaling.

Materials and methods

Rat spinal cord injury model. Adult female Sprague–Dawley (SD) rats were used. All animal experiments in this study were approved by the Animal Ethics Review Board of Jichi Medical University, and were performed in accordance with the Jichi Medical University Guide for Laboratory Animals and followed the principles of laboratory animal care formulated by the National Society for Medical Research.

Rats were anesthetized with an intraperitoneal injection of pentobarbital (40 mg/kg). Laminectomy of T9 was performed without disrupting the dura. Following laminectomy, a bilateral contusion injury was reliably created by delivering a 200 kdyn (2.00 N) force directly onto the spinal cord using an Infinite Horizon Impactor (Precision Systems and Instrumentation, MA). Following impaction, rats were maintained in a pathogen-free room under constant environmental control and subjected to twice-daily manual bladder expressions as necessary until urinary function returned.

Assisted stepping exercise for spinal cord injured rats. Spinal cord injured rats were subjected to assisted stepping exercise using the Rodent Robot 3000 (Robomedica, CA) robotic device [3]. This system consists of a motorized treadmill, a pair of robotic arms,

* Corresponding author. Fax: +81 285 44 5365.
E-mail address: eijikoba@jichi.ac.jp (E. Kobayashi).

0006-291X/$ - see front matter © 2009 Elsevier Inc. All rights reserved.
doi:10.1016/j.bbrc.2009.02.043